NASA / TM-2002-211673
ARL-TR-2725

Evaluation of Fatigue Crack Growth and Fracture Properties of Cryogenic Model Materials

John A. Newman
U.S. Army Research Laboratory
Vehicle Technology Directorate
Langley Research Center, Hampton, Virginia

Scott C. Forth
Langley Research Center, Hampton, Virginia

Richard A. Everett, Jr.
U.S. Army Research Laboratory
Vehicle Technology Directorate
Langley Research Center, Hampton, Virginia

James C. Newman, Jr.
Mississippi State University
Mississippi State, Mississippi

William M. Kimmel
Langley Research Center, Hampton, Virginia

May 2002

The NASA STI Program Office ... in Profile

Since its founding, NASA has been dedicated to the advancement of aeronautics and space science. The NASA Scientific and Technical Information (STI) Program Office plays a key part in helping NASA maintain this important role.

The NASA STI Program Office is operated by Langley Research Center, the lead center for NASA's scientific and technical information. The NASA STI Program Office provides access to the NASA STI Database, the largest collection of aeronautical and space science STI in the world. The Program Office is also NASA's institutional mechanism for disseminating the results of its research and development activities. These results are published by NASA in the NASA STI Report Series, which includes the following report types:

- TECHNICAL PUBLICATION. Reports of completed research or a major significant phase of research that present the results of NASA programs and include extensive data or theoretical analysis. Includes compilations of significant scientific and technical data and information deemed to be of continuing reference value. NASA counterpart of peer-reviewed formal professional papers, but having less stringent limitations on manuscript length and extent of graphic presentations.

- TECHNICAL MEMORANDUM. Scientific and technical findings that are preliminary or of specialized interest, e.g., quick release reports, working papers, and bibliographies that contain minimal annotation. Does not contain extensive analysis.

- CONTRACTOR REPORT. Scientific and technical findings by NASA-sponsored contractors and grantees.

- CONFERENCE PUBLICATION. Collected papers from scientific and technical conferences, symposia, seminars, or other meetings sponsored or co-sponsored by NASA.

- SPECIAL PUBLICATION. Scientific, technical, or historical information from NASA programs, projects, and missions, often concerned with subjects having substantial public interest.

- TECHNICAL TRANSLATION. English-language translations of foreign scientific and technical material pertinent to NASA's mission.

Specialized services that complement the STI Program Office's diverse offerings include creating custom thesauri, building customized databases, organizing and publishing research results ... even providing videos.

For more information about the NASA STI Program Office, see the following:

- Access the NASA STI Program Home Page at ***http://www.sti.nasa.gov***

- E-mail your question via the Internet to help@sti.nasa.gov

- Fax your question to the NASA STI Help Desk at (301) 621-0134

- Phone the NASA STI Help Desk at (301) 621-0390

- Write to:
  NASA STI Help Desk
  NASA Center for AeroSpace Information
  7121 Standard Drive
  Hanover, MD 21076-1320

NASA / TM-2002-211673
ARL-TR-2725

Evaluation of Fatigue Crack Growth and Fracture Properties of Cryogenic Model Materials

John A. Newman
U.S. Army Research Laboratory
Vehicle Technology Directorate
Langley Research Center, Hampton, Virginia

Scott C. Forth
Langley Research Center, Hampton, Virginia

Richard A. Everett, Jr.
U.S. Army Research Laboratory
Vehicle Technology Directorate
Langley Research Center, Hampton, Virginia

James C. Newman, Jr.
Mississippi State University
Mississippi State, Mississippi

William M. Kimmel
Langley Research Center, Hampton, Virginia

National Aeronautics and
Space Administration

Langley Research Center
Hampton, Virginia 23681-2199

May 2002

Available from:

NASA Center for AeroSpace Information (CASI)
7121 Standard Drive
Hanover, MD 21076-1320
(301) 621-0390

National Technical Information Service (NTIS)
5285 Port Royal Road
Springfield, VA 22161-2171
(703) 605-6000

Abstract

The criteria used to prevent failure of wind-tunnel models and support hardware were revised as part of a project to enhance the capabilities of cryogenic wind tunnel testing at NASA Langley Research Center. Specifically, damage-tolerance fatigue life prediction methods are now required for critical components, and material selection criteria are more general and based on laboratory test data. The suitability of two candidate model alloys (AerMet 100 and C-250 steel) was investigated by obtaining the fatigue crack growth and fracture data required for a damage-tolerance fatigue life analysis. Finally, an example is presented to illustrate the newly implemented damage tolerance analyses required of wind-tunnel model system components.

Introduction

A project to enhance the capabilities of the National Transonic Facility (NTF), a cryogenic wind tunnel at NASA Langley Research Center, was completed in September 2001. The goal of the NTF revitalization project was to improve the capabilities of the facility while reducing the costs and preparation time associated with cryogenic wind-tunnel tests. The overall project was broad, involving hundreds of researchers working on multiple individual tasks. The authors of this report updated the procedural guide used to prevent structural failure of model systems, *Wind-Tunnel Model Systems Criteria*, LAPG 1710.15 (ref. 1). The primary objectives of this task were to (1) provide material selection criteria to allow wind-tunnel model system components to be made from a broader range of alloys and (2) establish fatigue life criteria for critical wind-tunnel model system components based on the damage tolerance methodology.

Early in the development of the NTF, research was performed to identify and characterize a material suitable for wind-tunnel models and support hardware (ref. 2). Since the 1980s, NTF models and support hardware have been made from an 18%-Nickel maraging steel with a yield stress of 200 ksi (1380 MPa) (ref. 3), herein called C-200, with no effort to identify suitable alternate alloys. Although more advanced alloys have been developed during the 1980s and 1990s, model system components continued to use C-200 steel because it was easy to obtain, and evaluating new model alloys is expensive and time consuming. During the 1990s, it became difficult to acquire C-200 steel that met NTF non-destructive inspection (NDI) certification standards in desired quantities. Furthermore, recently developed wind-tunnel models are subjected to higher stresses to simulate the aerodynamics of modern high-performance aircraft, creating a need for model alloys with better performance. Alternate model alloys are needed that are easy to obtain in small quantities, meet NTF certification standards, and have better mechanical properties than C-200 over a wide range of testing temperatures (ref. 4).

The criteria used to prevent mechanical failure of wind-tunnel models and support hardware has recently been revised to allow the use of additional model alloys provided they pass the damage tolerance criteria. Damage tolerance life predictions are based on fatigue crack growth (FCG) and fracture test data, service loading conditions, and NDI results. All materials are assumed to contain crack-like defects that propagate under cyclic loading until reaching a critical crack size, where fracture occurs. Thus, fatigue life is equal to the number of cycles needed to propagate an initial flaw to the critical crack size (ref. 5). Non-destructive inspection (NDI) techniques are used to determine the initial flaw sizes, which are defined as the smallest crack that can be reliably detected (ref. 6). To simulate specific aerodynamic

conditions, wind-tunnel tests at the NTF are frequently performed at the cryogenic temperature of –171°C (–275°F) using liquid nitrogen (refs. 1-4). Therefore, model alloys must have desirable characteristics at both room temperature, 24°C (75°F), and –171°C. The objectives of this paper are to (1) present FCG and fracture data for two candidate model alloys (AerMet 100 and C-250 steels)* at ambient (24°C) and cryogenic temperatures (–171°C), and (2) give an example of the damage tolerance analyses needed to design wind-tunnel model system components.

Materials

Based on cost, availability, and fracture toughness data, two steel alloys were selected as potential candidates for wind tunnel models – AerMet 100 and C-250 steel (ref. 4). Both of these alloys (and the C-200 alloy they may replace) are categorized as maraging steels. Unlike other steels that are strengthened by carbon, maraging steels are precipitation strengthened near 480°C (900°F). The term "maraging" is derived from "martensitic-age-hardening" and denotes the precipitation age hardening of the low-carbon martensite matrix (ref. 7). The carbon-free precipitation hardening gives maraging steels several unique characteristics that other steels do not have. Maraging steel can be machined into components before hardening because the hardening processes results in little distortion. Also, maraging steels are well suited for welding and have fracture toughness values considerably higher than conventional steels. The chemical composition of AerMet 100 and C-250 steels are listed (as weight percent) in Table 1; values for C-200 are shown for comparison (ref. 6). C-250 and C-200 are similar in composition (17%-18% nickel, 7%-9% cobalt, 3%-5.2% molybdenum, and < 0.5% chromium). In comparison, AerMet 100 contains less nickel, and molybdenum (11%-12% nickel and 1.1%-1.3% molybdenum), and more cobalt and chromium (13%-14% cobalt and 2.9%-3.3% chromium) than the other alloys. AerMet 100 is strengthened by carbon, chromium, and molybdenum, while C-250 and C-200 are strengthened by cobalt, as indicated by the "C" in the alloy names (ref. 8). However, the mechanical properties of all three alloys (see Table 2) are similar (refs. 7-9).

Table 1. Chemical composition of cryogenic wind-tunnel model alloys in percent weight.

	AerMet 100	**C-250**	**C-200**
Nickel (Ni)	11% - 12%	17% - 19%	17% - 19%
Cobalt (Co)	13% - 14%	7% - 8.5%	8% - 9%
Molybdenum (Mo)	1.1% - 1.3%	4.6% - 5.2%	3.0% - 3.5%
Titanium (Ti)	< 0.015%	0.3% - 0.5%	0.15% - 0.25%
Aluminum (Al)	< 0.015%	0.05% - 0.15%	0.05% - 0.15%
Chromium (Cr)	2.9% - 3.3%	< 0.5%	< 0.2%
Copper (Cu)	trace	< 0.5%	< 0.2%
Manganese (Mn)	< 0.1%	< 0.1%	< 0.12%
Silicon (Si)	< 0.1%	< 0.1%	< 0.01%
Carbon (C)	0.21% - 0.25%	< 0.03%	< 0.03%
Phosphorous (P)	< 0.008%	< 0.01%	< 0.01%
Sulfur (S)	< 0.005%	< 0.01%	< 0.01%

Processing of Maraging Steels

Most maraging steels are air melted and then vacuum arc re-melted to produce a clean microstructure with low levels of impurities (*e.g.*, carbon and sulfur). Then the material is hot worked taking care to

* AerMet 100 is a registered trademark of Carpenter Steel. C-250 is commercially known as VascoMax C-250, a registered trademark of Teledyne Vasco.

ensure that elements such as titanium and carbon remain in solution; precipitation of Ti-C films at austenitic grain boundaries must be avoided. The material is then cold worked and machined prior to heat-treating. Maraging steels are normally solution annealed (austenitized) at temperatures near 900°C (1650°F) one hour per 25 mm (1 inch) of section thickness (ref. 9). Although maraging steels (including AerMet 100, C-250, and C-200 steels) are fully austenitic above 1350°F, higher annealing temperatures are used to ensure that the precipitations go into the solutions and all residual stresses are eliminated (ref. 9). On cooling, the austenite transforms into an iron-nickel martensite having a dense dislocation density but no twinning. The standard heat-treatment of 3 hours at 900°F achieves the peak hardness condition. AerMet 100 is annealed at 885°C ± 14°C (1625°F ± 25°F) for 60 minutes (+15 minutes/-0 minutes) in vacuum, followed by cooling to -73°C ± 8°C (-100°F ± 15°F) for 60 minutes ± 5 minutes, and aging at 482°C ± 6°C (900°F ± 10°F) for 6 hours (360 minutes) in vacuum. C-250 is annealed at 913°C (1675°F) for 60 minutes in vacuum, followed by aging at 482°C (900°F) for 3 hours (180 minutes) in vacuum. Both C-250 and C-200 steels are annealed and aged using the same time and temperature schedule.

Table 2. Room-temperature (and cryogenic) mechanical properties of cryogenic wind tunnel model alloys.

	AerMet 100	**C-250**	**C-200**
UNS designation	K92580	K92890	none
elastic modulus, E (Gpa)	194.4	195.3 (204.8)	193.7 (203.0)
yield stress, σ_y (MPa)	1724	1696 (2206)	1418 (1861)
ultimate stress, σ_u (MPa)	1965 (2495)	1792 (2275)	1461 (1930)
elongation (%)	13	8.5 (6)	11
reduction in area (%)	55	41 (25)	50
fracture toughness, K_{Ic} (MPa$\sqrt{m}$)	110	110 (44)	187 (86)
hardness (RC)	48-52	48-52	43-45
Charpy V Impact Energy (J)	34 (16)	28 (14)	49 (39)

Microstructure of Maraging Steels

The resulting microstructure of AerMet 100 and C-250 steels are shown in Figures 1a and 1b, respectively. Here, surfaces normal to the principal (orthogonal) material directions have been polished and etched to highlight microstructural features. These orthogonal micrographs have been arranged to appear as a three-dimensional cube of the material, herein termed orthogonal metallurgical cube. Micrographs are presented as orthogonal metallurgical cubes to better visualize the three-dimensional aspects of the materials microstructure. As seen in Figures 1a and 1b, both AerMet 100 and C-250 steels have fine microstructures (typical features less than 10 μm). Research has shown that grain-refinement of maraging steels increases the fracture toughness (ref. 10).

Experimental Testing and Results

Fatigue crack growth (FCG) and fracture data are needed to manage fatigue lives with damage tolerance methods. FCG and fracture tests were performed on AerMet 100 and C-250 steels, at 24°C and –171°C to determine which alloy is better suited for damage tolerance fatigue life management. All FCG and fracture data presented in this document are listed in tables in Appendix A.

Fatigue crack growth test methods

FCG tests were performed in accordance with ASTM standard E647 (ref. 11), using disk-shaped compact tension (DCT) specimens (ref. 12), shown schematically in Figure 2. The DCT specimen

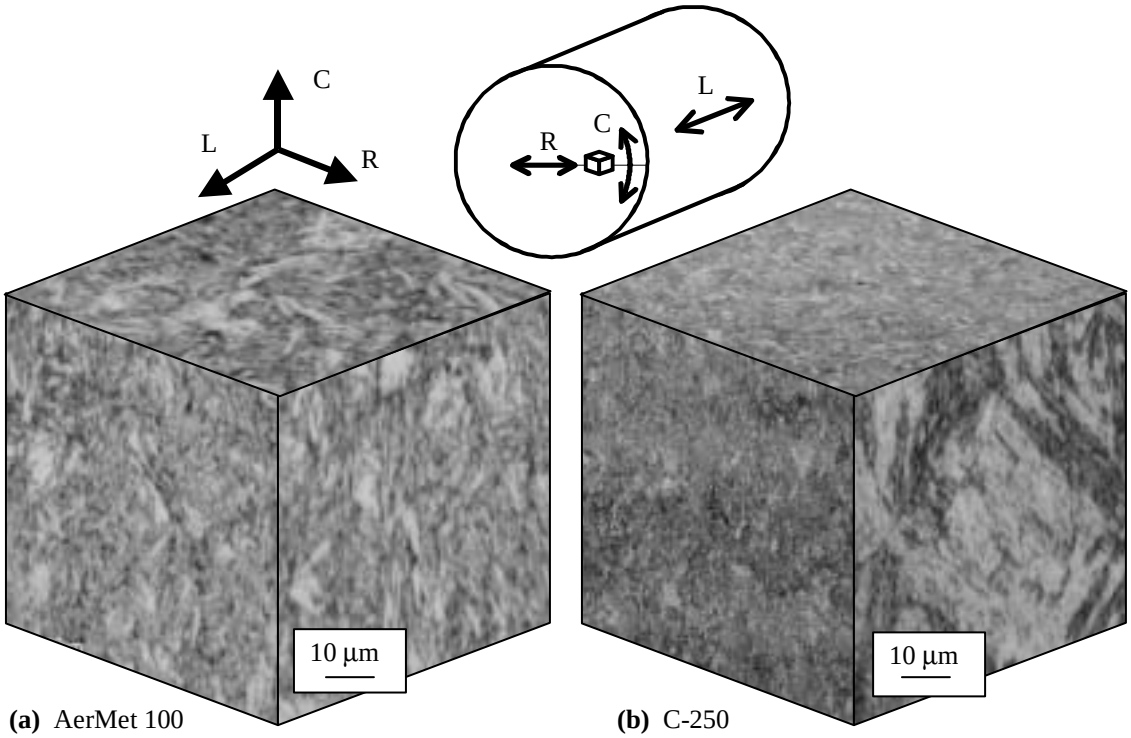

Figure 1. Micrographs of cryogenic model alloys arranged as metallurgical orthogonal cubes.

configuration was chosen because AerMet 100 and C-250 steel were obtained in round cylindrical bars of diameters 152 mm (6 inches) and 127 mm (5 inches), respectively. Specimens were made from cylindrical slices 25 mm (1 inch) thick. A photograph of typical AerMet 100 (left) and C-250 (right) specimens is shown in Figure 3. FCG tests were performed using computer-controlled servo-hydraulic test machines, where loads were applied to the specimens through the pinholes seen in Figures 2 and 3. Crack length was monitored during testing using crack-mouth compliance data, and loads were adjusted to achieve programmed stress intensity factors (ref. 13). Compliance-based crack length determinations were verified with visual measurements; FCG test data was corrected for the small differences (> 1%) between compliance-based and visual crack lengths. Two types of FCG tests were performed: (1) tests where the load ratio ($R = K_{min}/K_{max}$) was held constant as ΔK varied, called constant-R tests, and (2) tests where K_{max} was held constant and ΔK was reduced by increasing K_{min}, called constant-K_{max} tests. For the test data presented herein, ΔK varied at a constant value of C, defined in Equation 1,

$$C = \frac{1}{\Delta K}\left(\frac{d(\Delta K)}{d\,a}\right) \tag{1}$$

where a is the crack depth shown in Figure 2. All constant-K_{max} tests were performed with C = -787 m^{-1} (-20 in^{-1}); negative values of C indicate ΔK reduced during testing. Constant-R tests were performed at C = -78.7 m^{-1} (-2 in^{-1}) or C = +78.7 m^{-1} (+2 in^{-1}) for ΔK decreasing or ΔK increasing, respectively. FCG tests were performed in a room-temperature laboratory-air environment (24°C) or a cryogenic nitrogen environmental chamber at –171°C. Prior to testing, specimens were held at the specified temperature for at least 12 hours before testing to ensure steady-state thermal conditions were achieved.

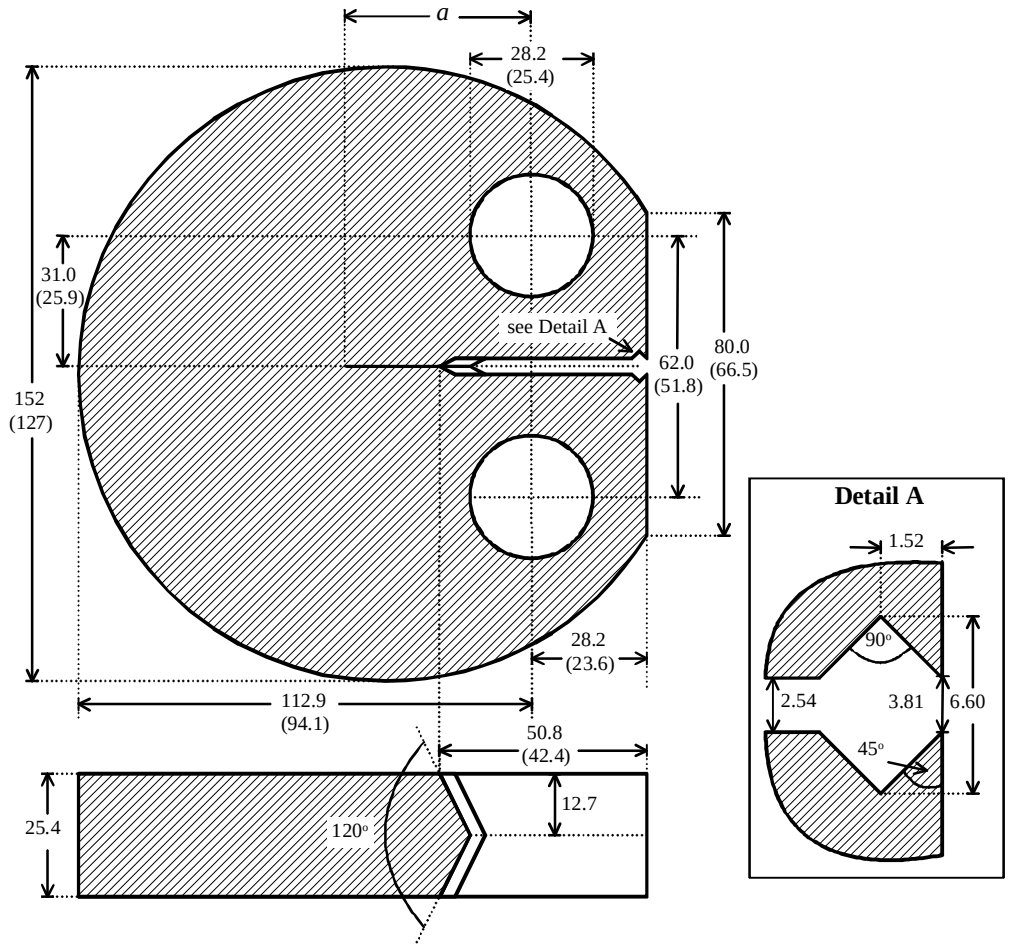

Figure 2. Disk-shaped compact tension (DCT) specimen. Dimensions are shown in mm for AerMet 100 specimens; where different, C-250 dimensions are shown in parentheses.

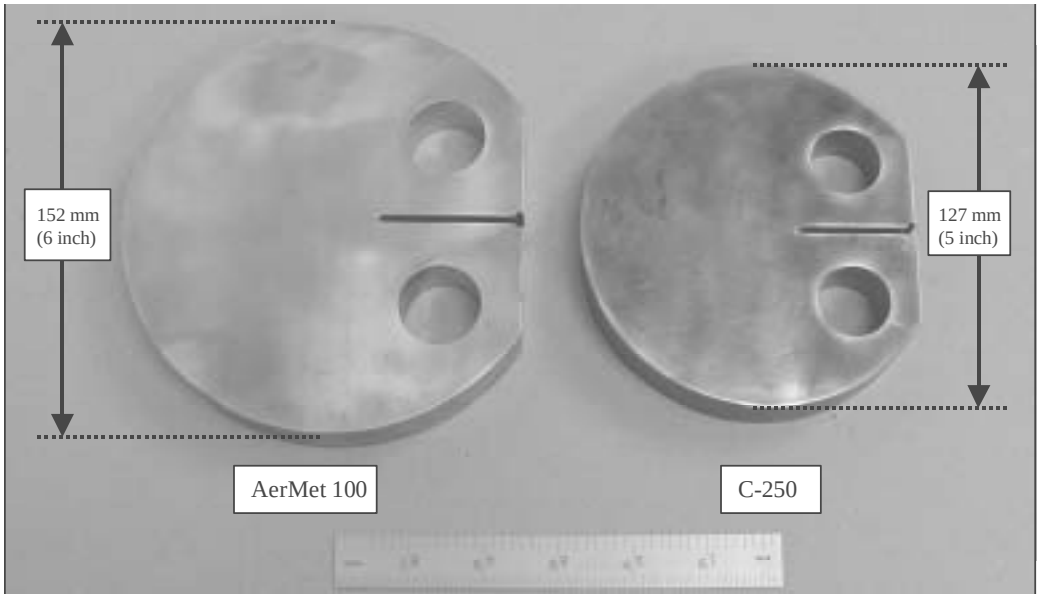

Figure 3. Photograph of DCT specimens for AerMet 100 (left) and C-250 (right).

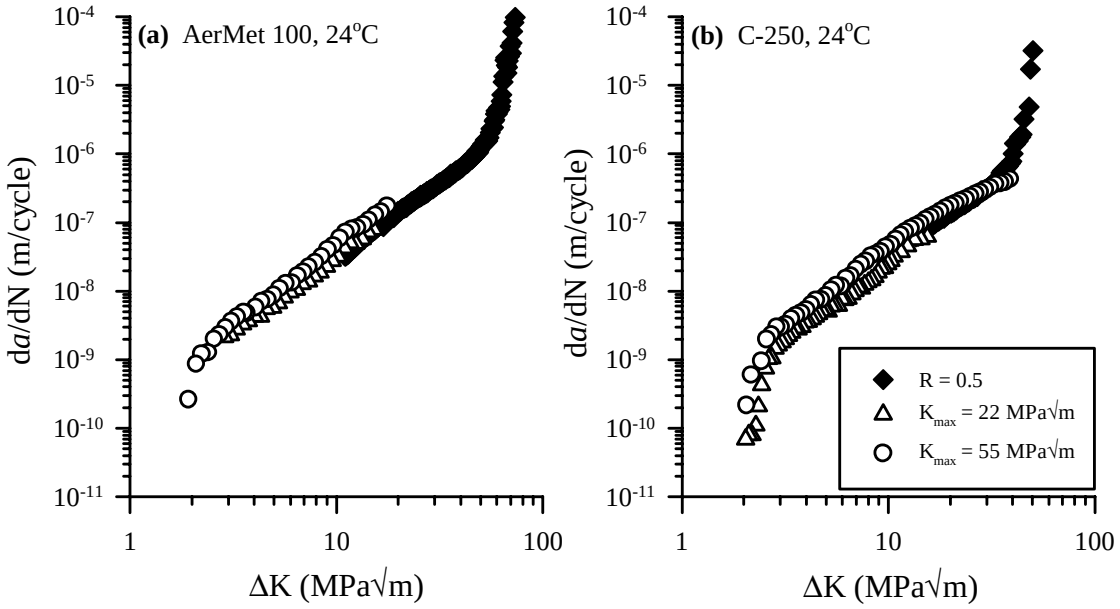

Figure 4. Room temperature (24°C) FCG data are plotted. (a) AerMet 100 data and (b) C-250 data.

Fatigue crack growth test results

FCG test data for AerMet 100 and C-250 steels at room temperature (24°C) are plotted as fatigue crack growth rate (d*a*/dN) versus ΔK in Figure 4. For both materials, constant-K_{max} data for 22 MPa√m and 55 MPa√m are shown as open triangular and open circular symbols, respectively. Constant-K_{max} tests were performed under decreasing-ΔK conditions (C = -787 m^{-1}) until reaching a d*a*/dN of approximately 10^{-10} m/cycle.[†] Constant-K_{max} tests produced fatigue crack growth thresholds, ΔK_{th}, approximately equal to 2.0 MPa√m, for both materials. Constant-R data are shown as solid diamond symbols for both alloys under increasing-ΔK conditions from approximately ΔK = 10 MPa√m to failure. For R = 0.5 increasing-ΔK conditions (C = +78.7 m^{-1}), failure occurred at ΔK values of approximately 73 MPa√m and 50 MPa√m for AerMet 100 and C-250, respectively.

FCG test data for AerMet 100 and C-250 steel tested at -171°C are plotted in Figure 5. For both materials, data are shown as open triangular and closed diamond symbols for constant-K_{max} = 22 MPa√m and constant-R = 0.5 test conditions, respectively. Constant-K_{max} tests were performed under decreasing-ΔK conditions (C = -787 m^{-1}), and constant-R = 0.5 tests were performed for both increasing-ΔK and decreasing-ΔK (C = +78.7 m^{-1} and –78.7 m^{-1}, respectively). For R = 0.5 increasing-ΔK conditions (C = +78.7 m^{-1}) at –171°C, failure occurred at ΔK values of approximately 20 MPa√m and 24 MPa√m for AerMet 100 and C-250, respectively. Constant-K_{max} = 55 MPa√m data could not be obtained at –171°C because of the low fracture toughness at this temperature.

The FCG data of both alloys are shown on the same plots in Figures 6a and 6b, for test temperatures of 24°C and –171°C, respectively. Data for AerMet 100 and C-250 are shown as open and solid circular symbols, respectively. In the FCG Paris regime (4 MPa√m < ΔK < 20 MPa√m), the differences between the sets of data are small at both temperatures. The solid line in both plots is a conservative bound on the

[†] The AerMet 100 constant-K_{max} = 22 MPa√m test was stopped at d*a*/dN = 2×10^{-9} m/cycle; however, the constant-K_{max} = 55 MPa√m test nearly achieved d*a*/dN = 10^{-10} m/cycle and would be a lower bound for any additional test data at K_{max} = 22 MPa√m.

data in the Paris regime; the equations of these lines are shown in the figures. As both alloys have similar FCG behavior in the Paris regime (at both temperatures) fracture properties will likely decide which alloy is best suited as a model material.

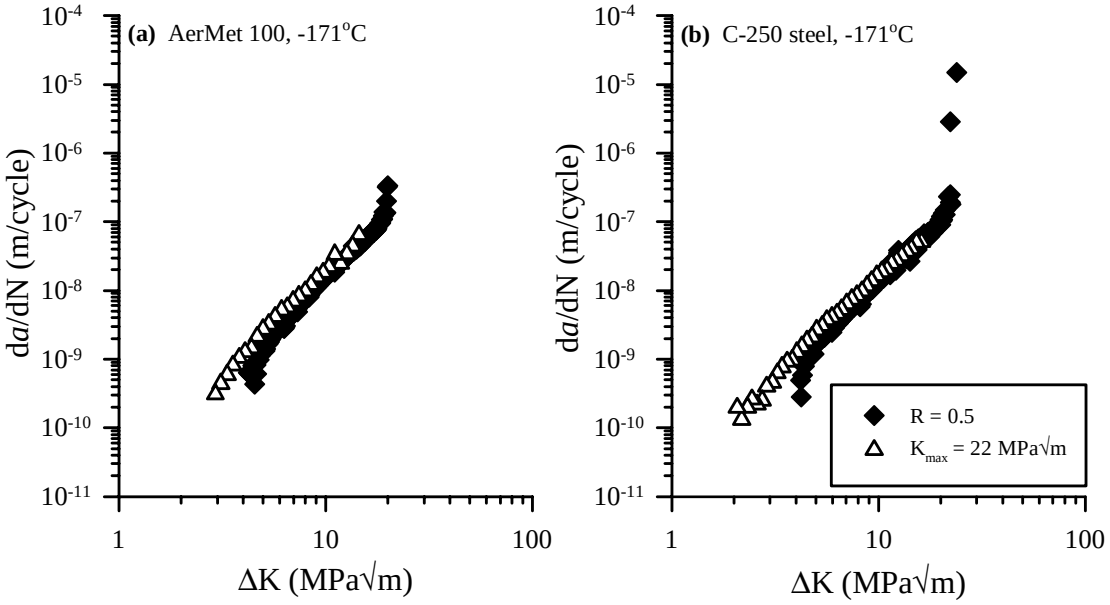

Figure 5. Cryogenic (-171°C) FCG data are plotted. (a) AerMet 100 data and (b) C-250 data.

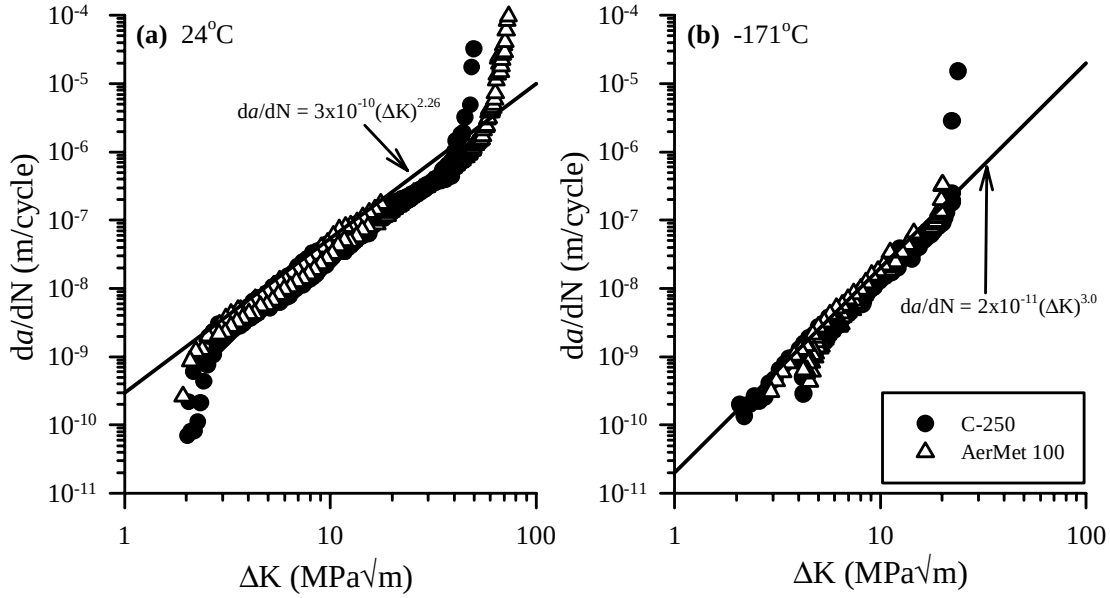

Figure 6. FCG data for both alloys are plotted for test temperatures of (a) 24°C and (b) –171°C.

Fracture testing

Fracture tests were performed on both AerMet 100 and C-250 at room temperature (24°C) and cryogenic test temperature (–171°C), using the DCT specimens shown in Figures 2 and 3, and the modified surface-crack tension (MSCT) specimens shown in Figure 7. For fracture testing with DCT

specimens, the majority of the crack front is under plane-strain conditions. For metallic materials, the plane-strain fracture toughness, K_{Ic}, is known to be a conservative value (*i.e.* K_{Ic} is the lowest value of fracture toughness), but in some cases this level of conservatism may be excessive. The MSCT specimen may provide more appropriate (and less conservative) fracture toughness values for cases where component failure is known to occur by fracture of surface cracks. As indicated in detail A of Figure 7, small surface cracks are defined by the crack depth, *a*, and the crack length, *c*, and are assumed to be semi-circular, *i.e.*, $c = a$. This specimen was essentially a flat dog-bone tensile specimen, 7.6 mm thick (0.30 inch) and 12.7 mm wide (0.50 inch) at the gage section. In the center of the gage section width, a small EDM (electro-discharge machining) notch was made $2c = 1.0$ mm (0.04 inch) long and $a = 0.5$ mm (0.02 inch) deep.

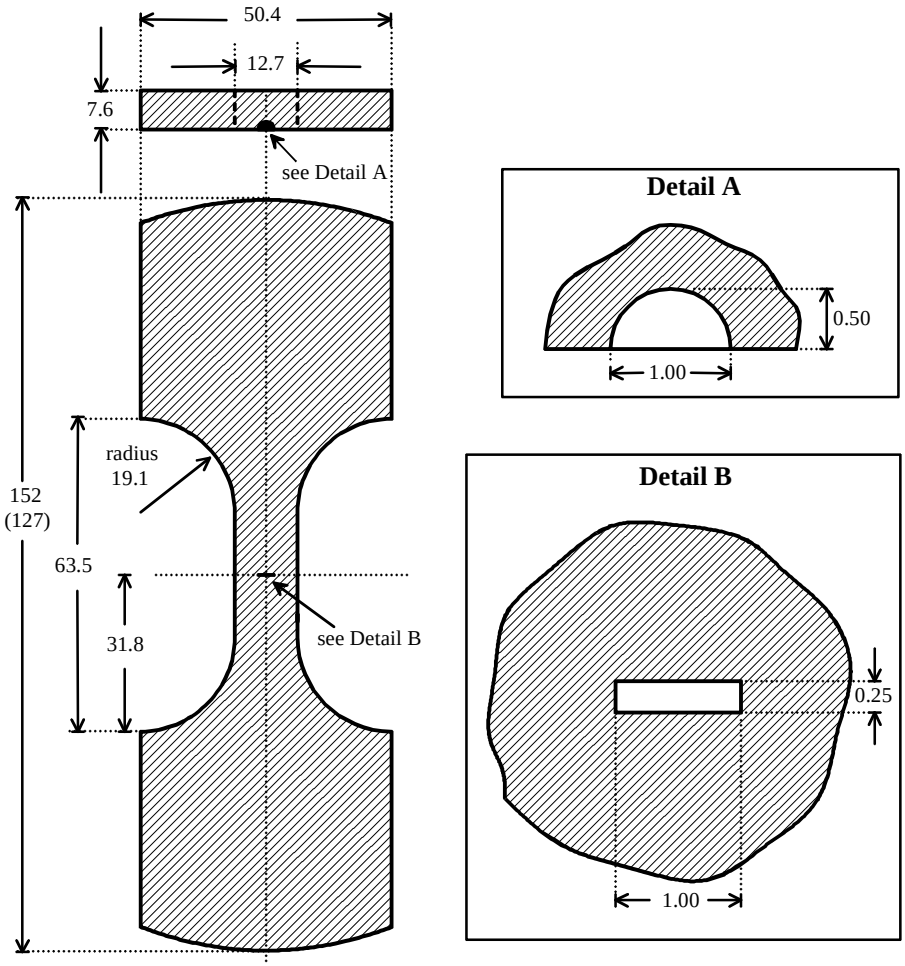

Figure 7. Modified surface-crack tension (MSCT) specimen. Dimensions shown in mm for AerMet 100 specimen; where different, C-250 dimensions are shown in parentheses.

Evaluation of long-crack specimen data

Fracture tests were performed in accordance with ASTM standard E399 using the DCT specimen configuration previously shown in Figures 2 and 3 (ref. 12). Specimens were pre-cracked by fatigue loading at room temperature in laboratory air. In all cases, fatigue pre-cracking was done with K_{max} values no greater than 50% of the specimen fracture toughness, and the normalized crack length at

fracture was 0.55 > *a*/W > 0.45. The specimen was then loaded at a stroke rate of 1.25 mm/minute (0.05 inches/minute) until failure occurred. Typical load and crack-mouth displacement data for test temperatures of 24°C and –171°C are plotted in Figures 8a and 8b for AerMet 100 and C-250, respectively. For these two tests, and for all other cases, the appropriate load to determine fracture toughness was the peak value (ref. 12).

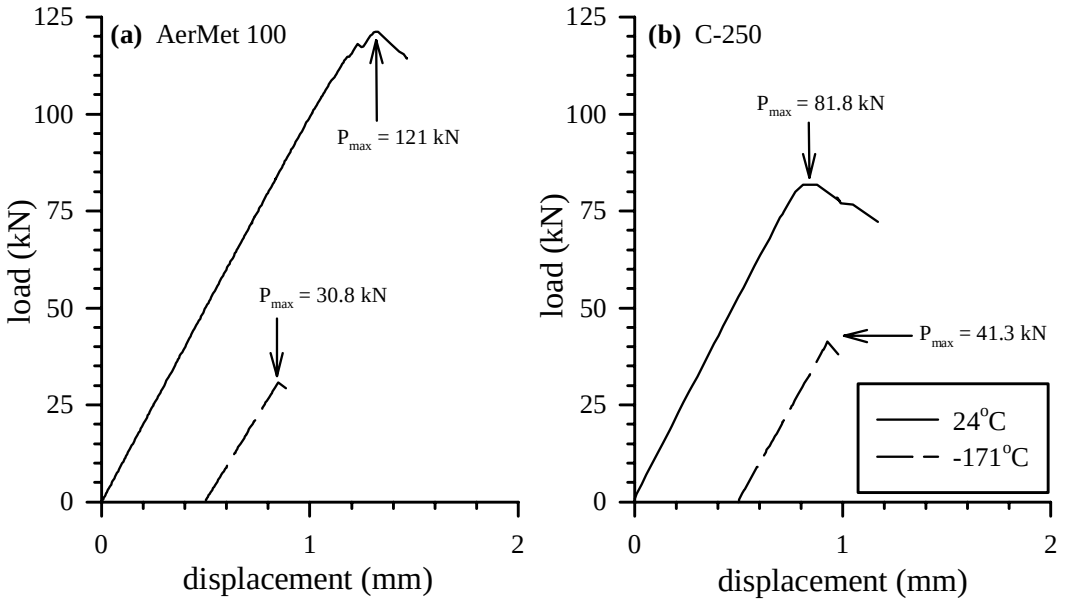

Figure 8. Load versus displacement data for DCT fracture tests are shown for (a) AerMet 100 and (b) C-250.

Photographs of typical DCT fracture surfaces for AerMet 100 are shown in Figures 9a and 9b, for test temperatures of 24°C and –171°C, respectively. Typical C-250 DCT fracture surfaces are shown in Figures 9c and 9d, for test temperatures of 24°C and –171°C, respectively. As noted in the photographs, specimens were pre-cracked under fatigue loading from the chevron crack starter notch. In each photograph a vertical dotted line indicates the final fatigue crack front where the specimen was fractured. It can be seen that the room-temperature fracture surfaces have more pronounced shear lips (Figures 9a and 9c) than those produced at cryogenic temperatures (Figures 9b and 9d). For cryogenic specimens, the shear lips near the specimen free surface are very small (cannot be seen in Figures 9b and 9d) indicating that both AerMet 100 and C-250 become brittle at cryogenic temperatures.

Fracture toughness data are shown in Figure 10 for AerMet 100 (shaded bars) and C-250 (solid bars) tested at temperatures of (a) 24°C and (b) –171°C. These data are given in Appendix A. The same scale is used on both plots to illustrate differences in fracture toughness at the two temperatures. The K_{Ic} values of AerMet 100 at 24°C are between 133 MPa√m and 125 MPa√m, approximately 40% greater than the corresponding K_{Ic} data for C-250 (between 84 MPa√m and 92 MPa√m). However, at –171°C the fracture toughness of C-250 ranges from 37 MPa√m to 51 MPa√m, on average nearly 10% greater than the corresponding data for AerMet 100 (ranging between 34 MPa√m and 47 MPa√m). Although AerMet 100 has a significant fracture toughness advantage at room temperature, C-250 has a slight fracture toughness advantage at –171°C.

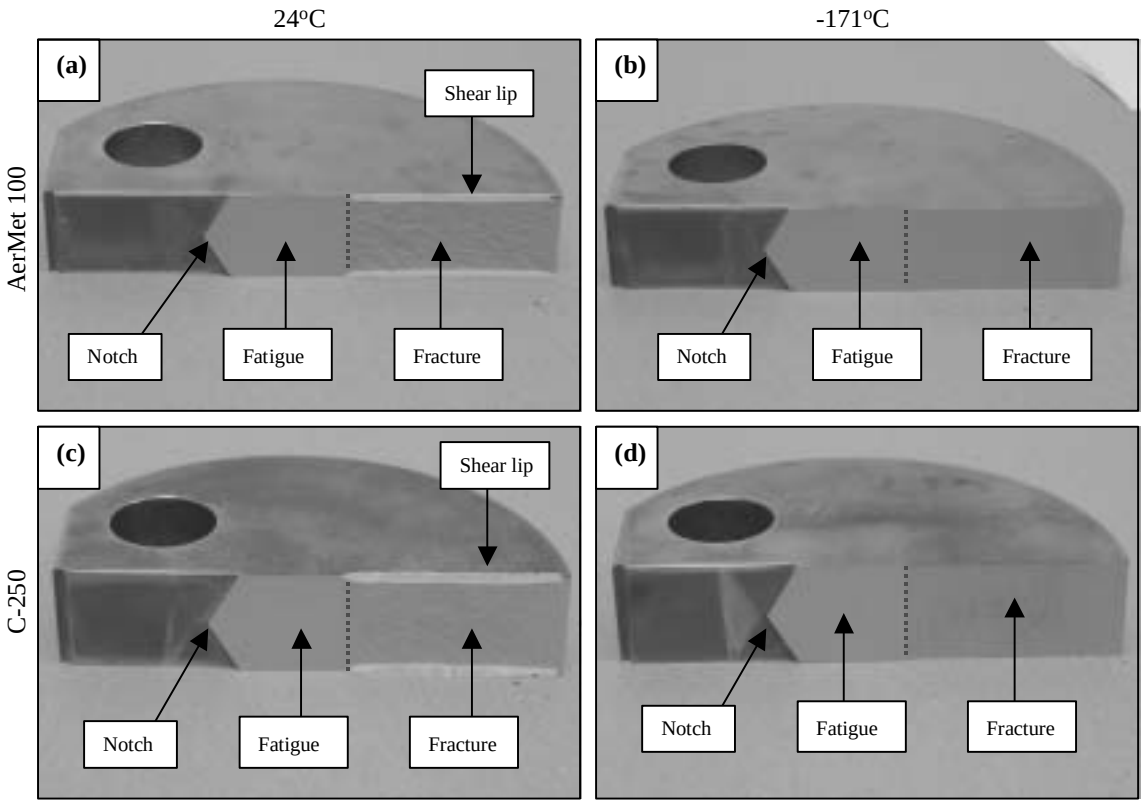

Figure 9. Photographs are shown of typical DCT specimen fracture surfaces. AerMet 100 specimens at (a) 24°C and (b) –171°C. C-250 specimens at (c) 24°C and (d) –171°C.

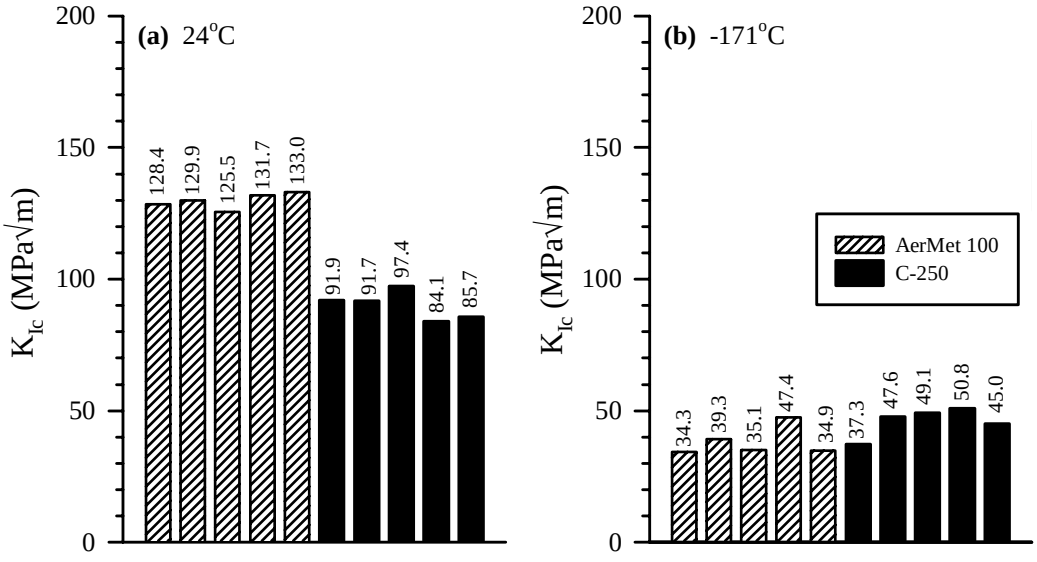

Figure 10. K_{Ic} data for both alloys at (a) 24°C and (b) -171°C

Small surface crack testing

For the DCT specimen fracture tests, the majority of the crack front was under plane-strain conditions. For metallic materials, the plane-strain fracture toughness, K_{Ic}, is the lowest value of fracture toughness.

This is significant because fracture analyses that use K_{Ic} as the fracture toughness value will give conservative results for any crack configuration. However, in some cases K_{Ic} may result in excessively conservative life predictions. For example, small surface cracks have higher fracture toughness values because they are affected by plane-stress surface conditions. For components that are known to fail by propagating surface cracks, it may be more appropriate to use fracture toughness values from small surface crack fracture tests.

Surface-crack fracture data was obtained using the modified surface-crack tension (MSCT) specimens shown schematically in Figure 7. This specimen configuration is similar to the surface-crack tension (SCT) specimen described by ASTM standards (ref. 14), but geometry changes were necessary because the material (AerMet 100 and C-250) was provided in cylindrical bar stock.[‡] One side of each specimen had a semi-circular EDM (electro-discharge machining) notch perpendicular to both the specimen surface and the loading axis, as seen in "Detail A" of Figure 7.

Specimens were cyclically loaded using closed-loop servo-hydraulic test machines to initiate a sharp fatigue crack at the EDM notch. Fatigue pre-cracking loads were held constant (P_{max} = 40 kN and R = 0.05) and crack length was measured periodically with a microscope. Fatigue pre-cracking was stopped once a crack reached its predetermined size (0.7 mm < c < 2.5 mm). Specimens were then loaded to failure at a displacement rate of 1.25 mm/minute (0.05 inches/minute). Typical load and displacement data acquired during testing are plotted in Figure 11 for (a) AerMet 100 and (b) C-250 at –171°C and 24°C. For all MSCT tests at 24°C, the gage section yielded before failure occurred.

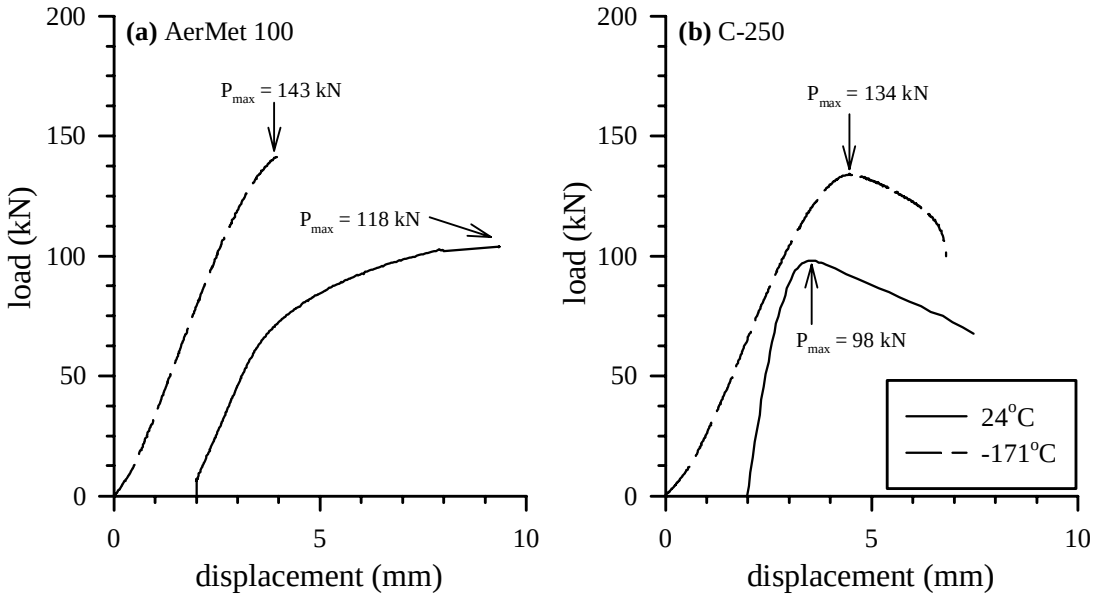

Figure 11. Load versus displacement data for MSCT fracture tests are shown for (a) AerMet 100 and (b) C-250.

Photographs of failed AerMet 100 and C-250 MSCT specimens are shown in Figures 12 and 13, respectively. The failure surfaces are shown at an angle and the EDM notch and fatigue crack are seen as

[‡] Although standard SCT specimens could have been made in the axial direction (of the cylindrical bar), the cracks in these specimens would not have the same orientation as the DCT specimens. Fracture toughness is known to vary with orientation, so comparing K_{Ic} with surface-crack fracture toughness values is only valid for a constant material orientation. A numerical analysis indicated the changes in specimen configuration did not significantly affect the fracture toughness values.

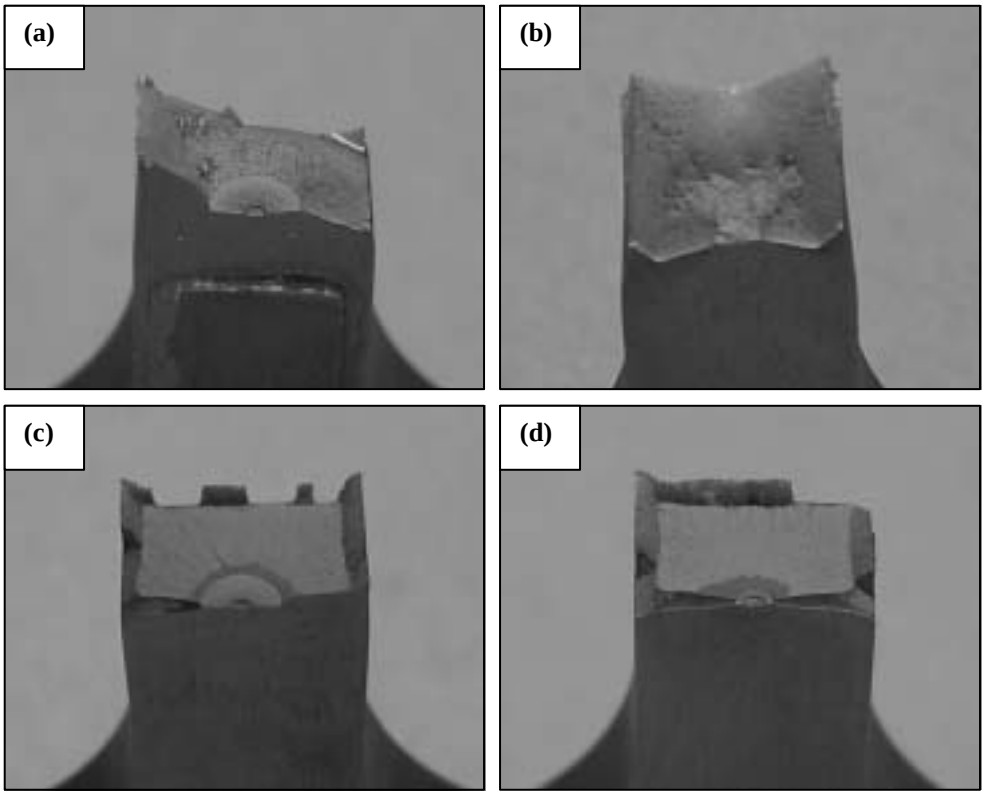

Figure 12. Photographs of AerMet 100 MSCT failure surfaces. (a) 24°C with large crack. (b) 24°C with small crack. (c) –171°C with large crack. (d) –171°C with small crack.

nearly semi-circular features starting at the midpoint of the specimen surface nearest the bottom of each photograph. Parts (a) and (b) correspond to a test temperature of 24°C, and parts (c) and (d) correspond to –171°C. Also, photographs on the left (parts (a) and (c)) and right (parts (b) and (d)) correspond to relatively large and small surface cracks (approximately a = 2.5 mm and a = 0.7 mm, respectively). For the AerMet 100 photographs in Figure 12, it can be seen that the failure surface of the room temperature specimens (Figures 12a and 12b) are angled approximately 45° from the loading axis, which is typical of ductile tensile failures. In contrast, the cryogenic failure surfaces (Figures 12c and 12d) are flat and smooth with small shear lips near the free surfaces, which is typical of brittle fracture failures. From the C-250 failure surfaces in Figure 13, it can be seen that both the room temperature (Figures 13a and 13b) and cryogenic specimens (Figures 13c and 13d) exhibit a failure surface typical of a ductile tension failure. However, the reduction in cross-sectional area of room temperature specimens is greater indicating that C-250 also exhibits reduced ductility at cryogenic temperatures, although this trend is less pronounced that for AerMet 100. Comparison of Figures 12a and 12b with Figures 13a and 13b indicates that C-250 is more ductile than AerMet 100 (based on a reduction in cross-sectional area) even at room temperature.

Room temperature MSCT test data are shown in Figure 14; the apparent fracture toughness, K_c, and the maximum gross stress are plotted as a function of c in parts (a) and (c), respectively. The K_c data shown in part (a) is calculated in terms of c and the peak load, using linear-elastic fracture mechanics assumptions. This is done even though linear-elastic fracture mechanics is not valid in some cases due to large-scale yielding. The maximum gross stress is calculated as the peak load divided by the pre-deformed cross-sectional area, nominally 97 mm^2 (0.15 in.^{2}). In Figure 14b, fracture data have been normalized with the plane-strain fracture toughness value, K_{Ic}. Recall from Figure 10 that K_{Ic} values for AerMet 100 and C-250 were approximately 125 MPa$\sqrt{m}$ and 85 MPa$\sqrt{m}$ at 24°C and 34 MPa$\sqrt{m}$ and 37

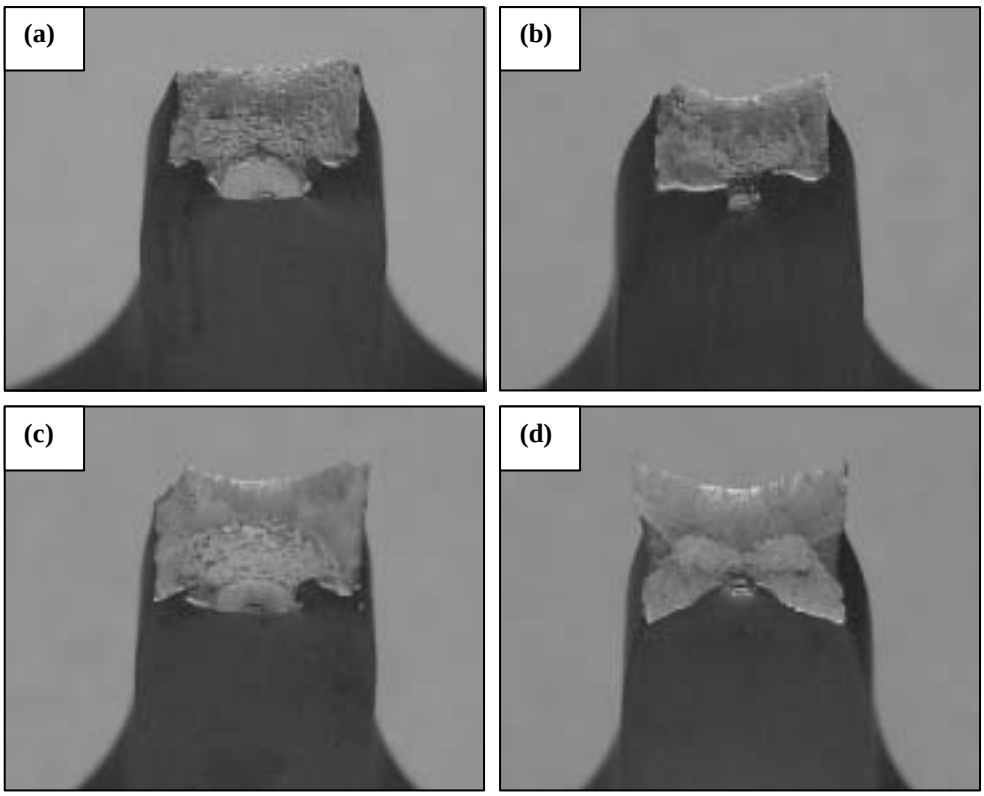

Figure 13. Photographs of C-250 MSCT failure surfaces. (a) 24°C with large crack. (b) 24°C with small crack. (c) –171°C with large crack. (d) –171°C with small crack.

MPa√m at –171°C, respectively. These data indicate that the apparent fracture toughness of these alloys is less than K_{Ic} at room temperature (due to yielding), but is significantly higher (as much as a 100% increase) than K_{Ic} at –171°C. In Figure 14d, the fracture stress has been normalized with the corresponding ultimate tensile stress (see Table 2). Here, it can be seen that the presence of the fatigue crack reduces the tensile stress capability of the specimens by approximately one-third; the magnitude of this reduction in load carrying capacity appears to be insensitive to the crack size.

Damage-Tolerance Life Predictions

On a microscopic level, most engineering alloys are inhomogeneous and have characteristic features (*e.g.*, grain boundaries and constituent particles) that are potential sites for cracks to initiate under fatigue loading and propagate to failure. The basis of the damage-tolerance methodology is that all structural components are assumed to contain crack-like flaws. Therefore, the fatigue life of a given component is the number of load cycles required to propagate a crack from an initial size to the critical size where fracture occurs. Damage-tolerance analysis is based on fracture mechanics concepts, which describe FCG rate in terms of the cyclic crack-tip stress intensity factor, ΔK,

$$\Delta K = F \cdot \Delta\sigma \sqrt{\pi a} \tag{2}$$

where a is the crack length, F is the geometry correction factor and $\Delta\sigma$ is the cyclic stress range defined as $\sigma_{max} - \sigma_{min}$ where max and min are the maximum and minimum stress levels (ref 15). It follows that $\Delta K = K_{max} - K_{min}$, where K_{max} corresponds to σ_{max} and K_{min} corresponds to σ_{min}. As seen from Equation 2, ΔK increases as a fatigue crack propagates (*i.e.*, a increases) under constant cyclic stress, $\Delta\sigma$. Eventually,

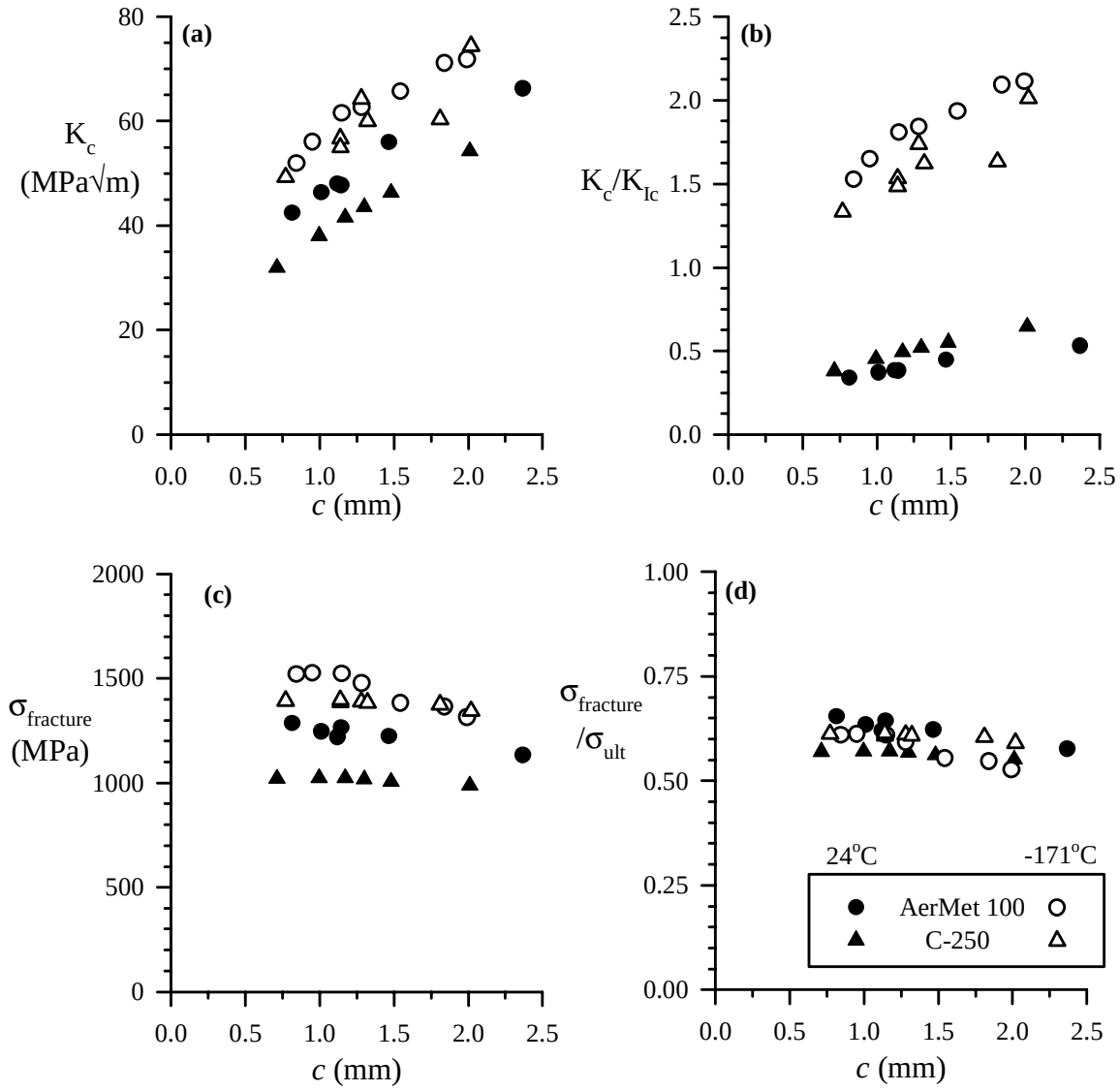

Figure 14. MSCT specimen fracture data are shown. (a) Fracture toughness data. (b) Normalized fracture toughness data. (c) Maximum stress during fracture tests. (d) Normalized maximum stress.

the crack-tip stresses increase until the maximum value of the stress intensity factor, K_{max}, exceeds the material fracture toughness, K_c. The critical crack length at fracture, a_c, is

$$a_c = \frac{1}{\pi}\left(\frac{K_c}{F\cdot \sigma_{max}}\right)^2 \tag{3}$$

where K_c is the fracture toughness and σ_{max} is the maximum stress value during fatigue loading. The fatigue life is determined as the number of load cycles required for the crack to propagate from an initial crack size, a_i, to the critical crack size, a_c. For most engineering alloys, the FCG rate, da/dN, can be related to ΔK (over a wide range of ΔK values) with the Paris power-law (ref. 16),

$$\frac{da}{dN} = C\cdot(\Delta K)^m \tag{4}$$

where C and m are material constants determined empirically from FCG test data. This power-law relationship can be integrated as follows (Equation 5) to determine fatigue life (ref. 17).

$$\int_{N_i}^{N_f} dN = \int_{a_i}^{a_f} \frac{d\,a}{C\cdot(\Delta K)^m} \tag{5}$$

ΔK is a function of crack length, a (Equation 2), so Equation 5 becomes,

$$\int_{N_i}^{N_f} dN = \int_{a_i}^{a_f} \frac{d\,a}{C\cdot\left(F\cdot\Delta\sigma\sqrt{\pi\,a}\right)^m} \tag{6}$$

The parameters C and m in Equation 6 are independent of crack length. The geometry correction factor F is a function of crack length, but in many cases F is nearly independent of crack length. To simplify fatigue-life calculations, F and $\Delta\sigma$ are assumed to be constant. Equation 6 can be integrated as,

$$\Delta N = \frac{a_f^{\left(1-m/2\right)} - a_i^{\left(1-m/2\right)}}{C\cdot\left(1-m/2\right)\cdot\left(F\cdot\Delta\sigma\sqrt{\pi}\right)^m} \tag{7}$$

where ΔN is the number of constant-amplitude load cycles required for a fatigue crack to propagate from an initial crack size, a_i, to a final crack size, a_f.[§] Equation 7 can be algebraically manipulated to determine the final crack length (a_f) in terms of the initial crack length (a_i), fatigue loading ($\Delta\sigma$ and ΔN), material parameters (C and m), and geometry (F),

$$a_f = \left[a_i^{\left(1-m/2\right)} + \Delta N\left(1-m/2\right)C\left(F\cdot\Delta\sigma\sqrt{\pi}\right)^m\right]^{\frac{1}{\left(1-m/2\right)}} \tag{8}$$

Fracture failure occurs when the crack length, a, reaches the critical crack size, a_c, (determined with Equation 3). The fatigue-life-to-failure, N_f, can be determined by replacing a_f in Equation 7 with the critical crack length, a_c, (Equation 3), as follows.

$$N_f = \frac{\left[\frac{1}{\pi}\left(\frac{K_c}{F\cdot\sigma_{max}}\right)^2\right]^{\left(1-m/2\right)} - \left[a_i\right]^{\left(1-m/2\right)}}{C\cdot\left(1-m/2\right)\cdot\left(F\cdot\Delta\sigma\sqrt{\pi}\right)^m} \tag{9}$$

Example of Damage-Tolerance Fatigue Analysis

An example is presented in this section to illustrate how the damage tolerance fatigue life methodology is used for wind tunnel applications. Consider a wind-tunnel structural component, made of AerMet 100 (σ_y = 1724 MPa) that is to be subjected to the polar stress history shown schematically in Figure 15. During each polar 40,000 vibratory load cycles occur at $\Delta\sigma_v$ = 20 MPa (at different values of load ratio, R) and the maximum stress is σ_{max} = 400 MPa. Although cyclic loading at lower R is

[§] Note that Equation 7 is not valid if m is exactly equal to 2.

potentially less damaging due to crack closure effects, this effect is neglected, to ensure conservative life predictions, by using closure-free FCG data. The load history of Figure 15 is *modeled* as 40,000 cycles at $\Delta\sigma_v$ = 20 MPa followed by one "ground-air-ground" load cycle at $\Delta\sigma_{GAG}$ = 400 MPa. Details of this load spectrum are listed in Table 3. The polar test history shown schematically in Figure 15 is typical of wind-tunnel tests where the angle-of-attack is periodically increased (ref. 4). The part in question is known to fail due to semi-circular surface cracks that propagate to failure under fatigue loading at cryogenic test temperatures (–171°C). Assume that the critical crack size is small compared to the size of the component and the assumption of a constant geometric correction factor, F = 0.73, is valid (ref. 15). For this component, the length of the smallest crack that NDI techniques can reliably detect is 1.0 mm (ref. 6).

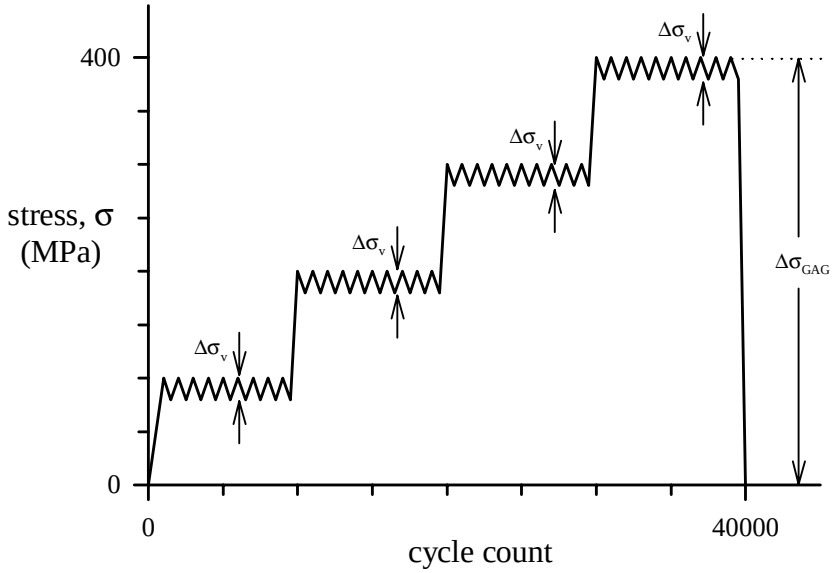

Figure 15. Idealized wind-tunnel polar spectrum.

Table 3. Loading input for Level 3 NASGRO analysis.

Number of Cycles	σ_{max} (MPa√m)	σ_{min} (MPa√m)
10,000	100	80
10,000	200	180
10,000	300	280
10,000	400	380
1	400	0

Damage-tolerance life prediction methods are more advanced than "safe-life" methods, and are best suited to prevent catastrophic fatigue failures (*i.e.*, where injury or substantial property damage would occur). However, damage-tolerance predictions are substantially more expensive and time consuming (compared to safe-life predictions) due to complex computations and required periodic crack inspections. However, this upfront expense can be offset via life extension programs inherent to damage tolerant designs, without the penalty of a fixed retirement time. To balance safety concerns with the need to reduce the costs associated with wind tunnel testing, damage-tolerance life prediction criteria have been made mandatory only for cryogenic and critically stressed model system components. Further, different

levels of damage tolerance analyses are available to model designers; higher analysis levels are less conservative and more complex. This multi-level analysis scheme was established to simplify the computational requirements (and cost) of DT life predictions while preserving safety. The first level, "level 1," is designed to be computationally simple, at the expense of excessive conservatism. Level 1 analyses use plane-strain fracture toughness, K_{Ic}, and a linear Paris FCG relation without threshold (*i.e.*, all load cycles cause damage). The next level, "level 2," allows an analyst to use either the FCG threshold, geometry-specific fracture toughness (*e.g.*, surface crack data), or both. A "level 3" analysis permits an analyst to determine fatigue life using a computer code, *e.g.*, NASGRO (ref. 18). For the example presented here, only level 1 and level 2 analyses are discussed.

Level 1 Analysis

A level 1 damage tolerance analysis allows fatigue crack growth and fracture data to be obtained from reliable sources in the open literature (refs. 19 and 20). However, the data presented in Figures 6b and 10b will be used for this example. Neglecting threshold, the fatigue crack growth relation and plane-strain fracture toughness (lower bound of data in Figure 10b) of this alloy at –171°C are expressed in Equations 10 and 11, respectively.

$$\mathrm{d}\,a/\mathrm{dN} = 2\times10^{-11}\cdot(\Delta\mathrm{K})^3 \tag{10}$$

$$\mathrm{K_{Ic}} = 34\,\mathrm{MPa}\sqrt{\mathrm{m}} \tag{11}$$

The critical crack size, at which failure occurs, can be expressed in terms of the fracture toughness and maximum applied stress, as shown in Equation 3. Here, F is a geometry correction factor, which is approximately 0.73 for a surface crack (ref. 15). In this example, fracture is assumed to occur when a crack grows to a length of 4.3 mm.

$$a_c = \frac{1}{\pi}\left(\frac{\mathrm{K_{Ic}}}{\mathrm{F}\cdot\sigma_{max}}\right)^2 = 4.3\,\mathrm{mm} \tag{12}$$

The fatigue life is the number of load cycles (or in this case polars) required to propagate the crack from the assumed initial crack size of 1.0 mm to the critical crack size of 4.3 mm. For the idealized polar shown schematically in Figure 15, Equation 8 must be evaluated twice per polar to determine the crack growth due to vibratory load cycles (Equation 13a) and the ground-air-ground cycle (Equation 13b).

$$a = \left[a^{\left(1-\mathrm{m}/2\right)} + \Delta\mathrm{N}\left(1-\mathrm{m}/2\right)\mathrm{C}\left(\mathrm{F}\cdot\Delta\sigma\sqrt{\pi}\right)^{\mathrm{m}}\right]^{\frac{1}{\left(1-\mathrm{m}/2\right)}} \tag{13a}$$

$$a = \left[a^{\left(1-\mathrm{m}/2\right)} + \left(1-\mathrm{m}/2\right)\mathrm{C}\left(\mathrm{F}\cdot\sigma_{max}\sqrt{\pi}\right)^{\mathrm{m}}\right]^{\frac{1}{\left(1-\mathrm{m}/2\right)}} \tag{13b}$$

For this example C = $2\text{x}10^{-11}$, m = 3, F = 0.73, a_i = 1.0 mm, a_f = 4.3 mm, $\Delta\sigma$ = 400 MPa, $\Delta\sigma_v$ = 20 MPa, and ΔN_v = 40,000 cycles were used. Iterative evaluation of Equations 13a and 13b predicts N_f to be 1974 polars. The computer code used to calculate the fatigue life for this example is shown in Appendix B. The total fatigue life prediction must be divided into no less than 4 inspection intervals to allow at least 3 inspections to find a propagating crack. For the predicted fatigue life of 1,974 polars, no more

than 493 polars may occur between crack inspections. If an inspection interval of 493 polars is acceptable, the component passes the level 1 analysis and is ready for testing with no need for additional analysis.

Level 2 Analyses

Suppose, the results of the example presented in the previous section were unacceptable. Failure to satisfy a level 1 analysis does not necessarily mean a given component cannot be safely used during wind tunnel testing. It may be that the level of conservatism associated with the level 1 analysis is too excessive. A level 2 analysis is more complex, but less conservative, and will be used to determine if components that failed to satisfy level 1 are safe for testing. Level 2 analyses eliminate conservatism by considering the effects of fatigue crack growth threshold, and increased fracture toughness due to specific crack geometries, *e.g.*, small surface cracks.

The FCG threshold, ΔK_{th}, is the minimum value of ΔK at which cracks will propagate. Thus, cyclic loads below ΔK_{th} can be neglected because they do not produce crack growth. To show the effect of threshold on fatigue life predictions consider a FCG threshold of ΔK_{th} = 2.0 MPa$\sqrt{m}$ and re-evaluate the example.[**] The vibratory loading that occurs during the polar ($\Delta\sigma_v$ = 20 MPa) can be neglected because the resulting ΔK has a maximum value of 1.7 MPa$\sqrt{m}$ (at failure for K_c = 34 MPa$\sqrt{m}$; a = 4.3 mm), which is less than ΔK_{th}. In this case, each polar is modeled as a single ground-air-ground load cycle of $\Delta\sigma_{GAG}$ = 400 MPa, as schematically shown in Figure 16, and the resulting fatigue life is calculated to be 11,842 polars. Considering FCG threshold resulted in a 500% increase in fatigue life.

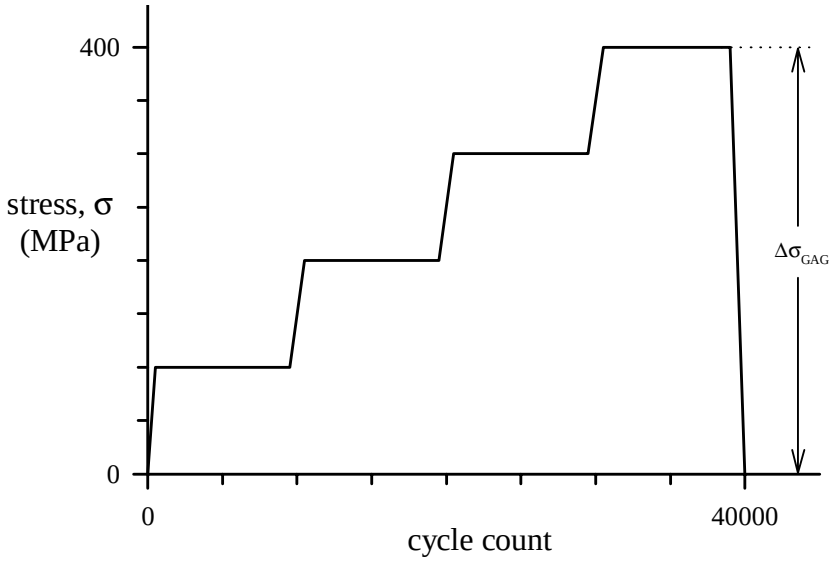

Figure 16. Idealized wind-tunnel polar load spectrum where vibratory loads are neglected.

Level 2 analyses permits using geometry-specific fracture toughness values. For this example (failure due to growth of small surface cracks at –171°C), the SCC data presented in Figure 14 is appropriate. If supported by test data, the *Wind Tunnel Model Systems Criteria* (ref. 1) allows fracture toughness values up to a 20% increase above K_{Ic}. For example, consider the AerMet 100 fracture data with a K_{Ic} = 34 MPa$\sqrt{m}$ and a MSCT fracture toughness of K_c = 60 MPa$\sqrt{m}$. Here, the maximum fracture toughness (K_c)

[**] Although not conclusively supported by the test data in Figure 5a, this assumption is made to demonstrate the effect of FCG threshold on damage-tolerance fatigue life predictions.

value available to an analyst is 41 MPa√m, a 20% increase in K_{Ic}. By using K_c = 41 MPa√m the predicted fatigue lives for the example increase to 2,287 polars, with no threshold, and 13,528 polars, for ΔK_{th} = 2 MPa√m.

Level 3 Analysis

Finally, assuming the Level 2 analysis does not provide an adequate life estimate for model implementation, a more complex FCG assessment may be permitted using computer codes. The NASGRO computer code is recommended for assessing the fracture mechanics life of NASA hardware. The required inputs for this code are component geometry, crack geometry, material and loading information. In this example, the initial crack will be 1.0 mm deep with an aspect ratio of 1.0, identical to the previous examples. The cross-section of the component is assumed to be large in comparison to the crack, so a rectangular body of 10 mm thick and 50.0 mm wide was chosen. The material was AerMet 100 with the properties defined in the NASGRO database such that σ_u = 1965 MPa, σ_y = 1724 MPa, K_c = 41 MPa√m, K_{Ic} = 34 MPa√m, A_k = 0.75, B_k = 1.0, C = 2.0x10^{-11}, n = 3.0, p = 0.25, q = 0.25, ΔK_0 = 2.9 MPa√m, C_{th+} = 0.1, C_{th-} = 0.1, R_{cl} = 0.7, α = 1.8 and S_{max}/S_{flow} = 0.3. The loading spectrum of Table 3 was used. The analysis was performed assuming no load interaction occurred. This is believed to be an appropriate assumption because load interaction effects are largely explained by crack closure effects (ref. 21), but for this example constant-K_{max} FCG test data was used that is not affected by closure (ref. 22). NASGRO was used to predict fatigue lives using the same values of fracture toughness (34 MPa√m and 41 MPa√m) and FCG threshold (0 and 2 MPa√m) used in the previous analyses. Neglecting FCG threshold, the level 3 results predict fatigue lives of 2,413 polars and 2,693 polars for fracture toughness values of 34 MPa√m and 41 MPa√m, respectively. Assuming a FCG threshold of ΔK_{th} = 2 MPa√m the predicted fatigue lives were 47,872 polars and 52,784 polars for fracture toughness values of 34 MPa√m and 41 MPa√m, respectively. The level 3 predictions are approximately 20% greater (less conservative) than the corresponding fatigue lives predicted from the level 1 and level 2 analyses.

Pitch Buffet Conditions

The polar load history, schematically shown in Figure 15, is typical of wind-tunnel tests where the angle-of-attack is incrementally increased. Increases in angle-of-attack will eventually cause aerodynamic instability, characterized by violent oscillatory loads, called pitch buffeting. Aerodynamic effects aside, a series of large oscillatory loads near the end of a test may dramatically shorten the fatigue life. Especially troubling is that the onset of pitch buffet conditions and the stresses that occur are not easily predicted. In cases where loads are not well known it is necessary for damage-tolerance life predictions to err on the conservative. As a practice it is recommended that a given component be able to survive the most severe pitch buffet conditions allowed with a comfortable margin of safety. Pitch buffet load conditions are idealized as shown schematically in Figure 17. For this example, consider that cyclic pitch buffet conditions result in 100 load cycles at $\Delta\sigma$ = 100 MPa and a maximum stress of 440 MPa. Here, each polar is modeled as 40,000 cycles at $\Delta\sigma$ = 20 MPa, 100 cycles at $\Delta\sigma$ = 100 MPa, and one cycle at $\Delta\sigma$ = 440 MPa. Assuming that every polar will result in pitch buffet conditions, fatigue failure is predicted to occur at 1,362 polars. Recall that the 40,000 vibratory load cycles are neglected if ΔK_{th} = 2.0 MPa√m is used; considering FCG threshold, failure is predicted to occur at 3,713 polars. Using a fracture toughness of K_c = 41 MPa√m, results in fatigue life calculations of 1,623 polars with no FCG threshold, and 4,426 polars using ΔK_{th} = 2.0 MPa√m. By considering bitch buffeting, the predicted fatigue lives are decreased by approximately 30% where no FCG threshold is assumed, and by approximately 70% where ΔK_{th} = 2 MPa√m is assumed. Level 3 life predictions were also made for pitch buffet conditions. Neglecting FCG threshold, the level 3 results predict fatigue lives of 1,741 polars and 2,006 polars for fracture toughness values of 34 MPa√m and 41 MPa√m, respectively. Assuming a FCG threshold of ΔK_{th}

= 2 MPa√m the predicted fatigue lives were 6,972 polars and 8,133 polars for fracture toughness values of 34 MPa√m and 41 MPa√m, respectively. The level 3 predictions were between 20% and 100% greater (less conservative) than the corresponding level-1 and level-2 fatigue life predictions.

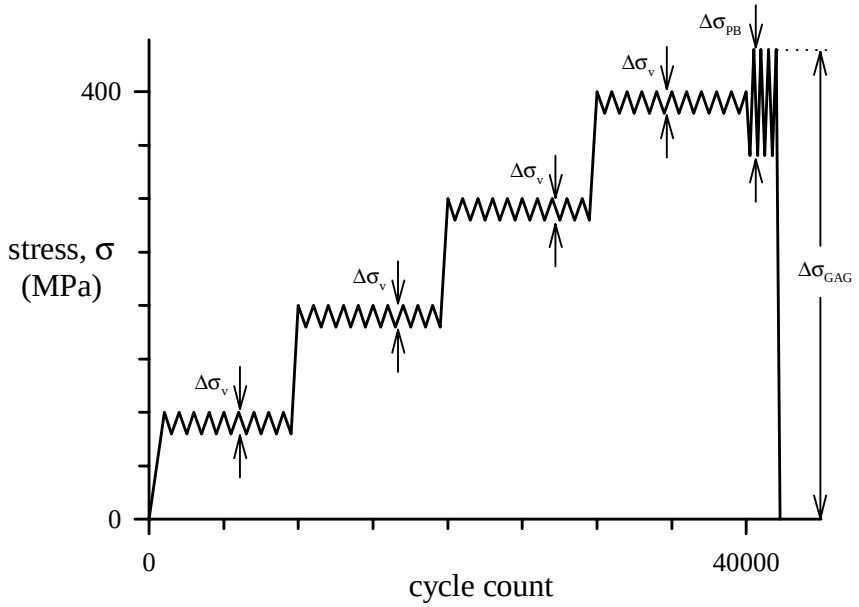

Figure 17. Idealized wind-tunnel polar load spectrum including pitch buffeting.

Discussion

Damage-tolerance fatigue life predictions are calculated as the number of load cycles required for a fatigue crack to propagate from an initial size to fracture. Multiple crack inspections are required during this fatigue life to ensure any fatigue crack would be detected before failure occurs. If no cracks are found during an inspection, the smallest crack that can be reliably detected is assumed to exist to ensure fatigue life predictions are conservative, *i.e.*, predicted fatigue lives are less than actual fatigue lives. The complex nature of fatigue crack growth and fracture behavior necessitates the use of simplifying approximations (*e.g.*, FCG power-law relation of Equation 10) to make damage-tolerance life calculations manageable. Unfortunately, using idealized material behavior decreases the accuracy of fatigue life predictions. Because errors are unavoidable, it is important that all simplifying approximations result in conservative fatigue life predictions. The damage-tolerance fatigue life criteria used for wind-tunnel model system components uses a multi-level analysis scheme where an analyst may choose the appropriate level of complexity/conservatism. This report is loosely divided into two sections, one focused on acquiring the experimental data needed for damage-tolerance life predictions and the other demonstrating how damage-tolerance life predictions are made using these experimental results. The methods used to ensure conservatism are discussed in the following paragraphs.

Experimental Testing

As damage-tolerance life predictions are based on experimental data, it is important that this data is appropriate for the material and expected service conditions, and that any simplifying assumptions are always conservative. Fatigue crack growth rates are normally expressed as a function of ΔK, although load ratio (R = minimum load/maximum load) is also known to affect da/dN, *i.e.*, fatigue crack growth rates increase with increasing R. Most load ratio effects are due to crack closure – contact of crack faces

during cyclic loading (ref. 21). A simplified, yet conservative, relation between d*a*/dN and ΔK should be based on closure-free FCG data. For this reason all FCG data was obtained at either R = 0.5 (where closure effects are minimal) or with constant-K_{max} testing (where no closure occurs). Constant-K_{max} test data is especially recommended to determine ΔK_{th} because near-threshold closure behavior is complex (ref. 22). Low-R laboratory threshold data may produce values of ΔK_{th} that are non-conservative for high R fatigue loading (refs. 23-25). Even slight changes in ΔK_{th} may have a dramatic effect on fatigue life.

Where possible, it is recommended that fatigue life calculations be made using the plane-strain fracture toughness, K_{Ic}, because it is conservative. (Recall that the results of Figure 14 showed that K_{Ic} was inappropriate at high stresses where large-scale yielding occurs.) In cases where failure is known to result from cracks of a specific geometry (*e.g.*, surface cracks), test data appropriate for that crack configuration may be used (up to a 20% increase in fracture toughness). However, it is the responsibility of the analyst to know the geometric crack configuration and any increases in the fracture toughness must be supported by test data, *i.e.*, any increase in fracture toughness due to a known surface crack configuration is only permitted if supported by data.

Fatigue Life Predictions

Interpretation of experimental data is an important step in the damage-tolerance analysis process. Simplifications must be made with conservatism in mind. For example, when approximating the Paris regime FCG data in Figure 6, the curve chosen was a conservative bound on the available data rather than a "best fit." For fracture data, the lowest value of fracture toughness is used to ensure conservative predictions and account for statistical variations (*i.e.*, scatter) in experimental data.

For the example presented in the "Damage Tolerance Life Predictions" section of this report, the predicted fatigue lives are shown in Table 4. For this example, a 20% increase in fracture toughness resulted in an increase in fatigue life of approximately 20%. Predicted fatigue lives increased by approximately 500% for no pitch buffeting, and approximately 200% with pitch buffeting, by considering FCG threshold. For this example, predicted fatigue lives were more affected by the FCG effects (compared with fracture toughness effects) because the load history included many small amplitude load cycles that were below the FCG threshold. For other load histories, fatigue life predictions may be affected more by the fracture toughness than ΔK_{th}. The fatigue life predictions listed in Table 4 vary by a factor of 6 depending on the assumptions used to perform the damage-tolerance calculations. It is important to note that the actual fatigue life would be greater than all of the predictions because all

Table 4. Summary of damage-tolerance fatigue life predictions.

Analysis Level	K_c (MPa$\sqrt{m}$)	ΔK_{th} (MPa$\sqrt{m}$)	N_f (no pitch buffet)	N_f (pitch buffet)
Level 1	34	0	1,974 polars	1,362 polars
Level 2	41	0	2,287 polars	1,623 polars
Level 2	34	2	11,842 polars	3,713 polars
Level 2	41	2	13,528 polars	4,426 polars
Level 3	34	0	2,413 polars	1,741 polars
Level 3	41	0	2,693 polars	2,006 polars
Level 3	34	2	47,872 polars	6,972 polars
Level 3	41	2	52,784 polars	8,133 polars

approximations made for material behavior are conservative. However, if the results of a level 1 analysis are acceptable there is no need to perform more complex, and less conservative, analyses. Analysts should be aware that increasingly complex and less conservative analysis methods require an increased level of technical expertise. Non-experts are warned against performing advanced analyses and interpreting experimental results because mistakes may result in non-conservative fatigue life predictions and potentially catastrophic failure. Further, life predictions made by experts may be non-conservative if the assumptions used by the analysis are incorrect, *e.g.*, if the service loading is more severe than anticipated or if pitch buffet conditions are ignored.

Conclusions

In this report, fatigue crack growth fracture data are presented for AerMet 100 and C-250 steel, two candidate alloys for wind-tunnel model systems. These data are needed to perform the required damage-tolerance life calculations to ensure safe operating conditions at either room temperature (24^{o}C) or cryogenic test temperature (–171^{o}C). An example is presented to illustrate how damage-tolerance fatigue life calculations are made to ensure safe operating conditions for wind-tunnel model systems. This example was designed to illustrate the multi-level nature of the newly revised wind-tunnel model systems criteria procedural guide.

References

1. *Wind Tunnel Model Systems Criteria*, LAPG 1710.15, NASA Langley Research Center, September 2000.

2. R. L. Tobler, "Materials Studies for Cryogenic Wind Tunnels," National Bureau of Standards, NBSIR 79-1624, 1980.

3. J. A. Wagner, "Mechanical Behavior of 18-Ni 200 Grade Maraging Steel at Cryogenic Temperatures," Proceedings of the 26th Structures, Structural Dynamics and Materials Conference, 15-17 April 1985, Orlando, Florida, pp. 385-390.

4. W. M. Kimmel, J. A. Newman, N. S. Kuhn, and R. F. Berry, "Cryogenic Model Materials," Proceedings of the 39th AIAA Aerospace Sciences Meeting and Exhibit, January 8-11, 2001, Reno, Nevada, AIAA-2001-0757.

5. R. A. Everett and W. Elber, "Damage Tolerance Issues Related to Metallic Rotorcraft Dynamic Components," *Journal of the American Helicopter Society*, Vol. 45, pp. 3-10.

6. D. Thomas, *Fracture Control Requirements for Space Station*, NASA SSP 30558, Rev. B, 1994.

7. *Metals Handbook*, 9th Edition, *Volume 1, Properties and Selections: Irons and Steels*, B. P. Bardes, Editor, American Society for Metals, 1978, Metals Park, Ohio.

8. A. M. Hall and C. J. Slunder, "The Metallurgy, Behavior, and Application of the 18-Percent Nickel Maraging Steels," 1969, NASA SP-5051.

9. *Aerospace Structural Handbook*, 1995 Edition, W. F. Brown, H. Mindlin, and C. Y. Ho, Editors, CINDAS/USAF CRDA Handbooks Operation, Purdue University, West Lafayette, Indiana.

10. H. F. Rush, "Grain Refinement of High Strength Steel to Improve Cryogenic Toughness," AIAA Paper Number 85-0749.

11. "Standard Test Method for Measurement of Fatigue Crack Growth Rates," *Annual Book of ASTM Standards*, Vol. 3.01, E647, American Society for Testing and Materials, West Conshohocken, PA, 2001.

12. "Standard Test Method for Plane-Strain Fracture Toughness of Metallic Materials," *Annual Book of ASTM Standards*, Vol. 3.01, E399, American Society for Testing and Materials, West Conshohocken, PA, 2001.

13. A. Saxena, S. J. Hudak, J. K. Donald, and D. W. Schmidt, "A Computer Controlled Decreasing Stress Intensity Technique for Low Rate Fatigue Crack Growth Testing," *Journal of Testing and Evaluation*, Vol. 6, 1978, pp. 167-174.

14. "Standard Practice for Fracture Testing with Surface-Crack Tension Specimens," *Annual Book of ASTM Standards*, Vol. 3.01, E740, American Society for Testing and Materials, West Conshohocken, PA, 2001.

15. J. C. Newman, Jr. and I. S. Raju, "Stress-Intensity Factor Equations for Cracks in Three-Dimensional Finite Bodies Subjected to Tension and Bending Loads," *Computational Methods in the Mechanics of Fracture*, S. N. Atluri, Editor, Elsevier Science Publishers, 1986, New York, NY.

16. P. Paris and F. Erdogan, "A Critical Analysis of Crack Propagation Laws," *Journal of Basic Engineering*, Transactions of the ASME, December, 1963, pp.528-534.

17. N. E. Dowling, *Mechanical Behavior of Materials*, 2nd edition, Prentice Hall, 1999, Upper Saddle River, NJ.

18. NASGRO, Computer software available online at http://mmptdpublic.jsc.nasa.gov/nasgro/nasgromain.html, NASA Johnson Space Center, 2000.

19. C. M. Hudson and S. K. Seward, "A Compendium of Sources of Fracture Toughness and Fatigue Crack Growth Data for Metallic Alloys," *International Journal of Fracture*, Vol. 14, 1978, pp. R151-R184.

20. C. M. Hudson and S. K. Seward, "A Compendium of Sources of Fracture Toughness and Fatigue Crack Growth Data for Metallic Alloys – Part II," *International Journal of Fracture*, Vol. 20, 1982, pp. R57-R117.

21. R. Hertzberg, W.A Herman, T. Clark and R. Jaccard, "Simulation of Short Crack and Other Low Closure Loading Conditions Utilizing K_{max} ΔK-Decreasing Fatigue Crack Growth Procedures," *Small Crack Test Methods*, ASTM STP 1149, ASTM, 1991, pp. 197-220.

22. J. C. Newman, Jr. and W. Elber, Editors, *Mechanics of Fatigue Crack Closure, ASTM, STP 982*, 1988, American Society for Testing and Materials, Philadelphia, Pennsylvania.

23. J. K. Donald, G. H. Bray, and R. W. Bush, " Introducing the K_{max} Sensitivity Concept for Correlating Fatigue Crack Growth Data," *High Cycle Fatigue of Structural Materials*, The Minerals, Metals, and Materials Society, 1978, pp. 123-141.

24. J. A. Newman and R. S. Piascik, "Plasticity and Roughness Closure Interactions Near the Fatigue Crack Growth Threshold," *Fatigue and Fracture Mechanics: 33rd Volume, ASTM STP 1417*, W. G. Reuter and R. S. Piascik, Editors, American Society for Testing and Materials, West Conshohocken, Pennsylvania, 2002.

25. J. C. Newman, Jr., "Analyses of Fatigue Crack Growth and Closure Near Threshold Conditions for Large-Crack Behavior," *Fatigue Crack Growth Thresholds, Endurance Limits, and Design, ASTM STP 1372*, J. C. Newman, Jr. and R. S. Piascik, Editors, American Society for Testing and Materials, West Conshohocken, PA, 2000, pp. 227-251.

Appendix A

The fatigue crack growth data (d*a*/dN and ΔK) plotted in Figures 4 through 6 are listed in Tables A1 through A10 of this appendix. The DCT fracture data of Figure 10 are listed in Table A11, and the MSCT fracture data of Figure 14 are listed in Tables A12 and A13. Fatigue pre-cracking information is provided with the fracture data. For the DCT data final values of K_{max}, P_{max} (maximum load applied to the specimen), *a* (crack length), and *a*/W (normalized crack length) are listed. For the MSCT data final values of K_{max}, P_{max} (maximum load applied to the specimen), σ_{max} (maximum gage-section stress) *a* (crack depth), and *c* (crack length) are listed.

Table A1. Constant-K_{max} FCG data for AerMet 100 at 24°C.

K_{max} = 22 MPa√m				K_{max} = 55 MPa√m			
ΔK (MPa√m)	d*a*/dN (m/cycle)	ΔK (MPa√m)	d*a*/dN (m/cycle)	ΔK (MPa√m)	d*a*/dN (m/cycle)	ΔK (MPa√m)	d*a*/dN (m/cycle)
15.22	8.00E-08	4.92	5.79E-09	17.61	1.74E-07	5.69	1.29E-08
14.29	7.18E-08	4.58	5.50E-09	16.50	1.43E-07	5.31	1.09E-08
13.39	5.72E-08	4.29	4.29E-09	15.42	1.29E-07	4.97	8.72E-09
12.47	4.88E-08	4.03	4.31E-09	14.42	1.09E-07	4.64	7.57E-09
11.69	5.05E-08	3.76	3.63E-09	13.54	9.27E-08	4.35	7.03E-09
10.93	4.23E-08	3.52	3.25E-09	12.63	8.39E-08	4.06	5.80E-09
10.21	3.22E-08	3.29	2.79E-09	11.85	8.01E-08	3.67	4.75E-09
9.58	2.74E-08	3.08	2.29E-09	11.09	7.25E-08	3.56	4.86E-09
8.95	2.29E-08	2.87	2.16E-09	10.37	5.92E-08	3.31	4.19E-09
8.37	1.88E-08			9.69	4.61E-08	3.10	3.60E-09
7.82	1.63E-08			9.06	4.00E-08	2.90	2.94E-09
7.34	1.40E-08			8.49	3.19E-08	2.72	2.31E-09
6.84	1.26E-08			7.91	2.60E-08	2.55	2.01E-09
6.40	1.06E-08			7.36	2.24E-08	2.39	1.27E-09
5.98	9.67E-09			6.92	1.88E-08	2.22	1.21E-09
5.60	8.14E-09			6.48	1.68E-08	2.09	8.68E-10
5.25	6.70E-09			6.07	1.32E-08	1.93	2.63E-10

Table A2. Constant-K_{max} = 22 MPa√m fatigue crack growth data for AerMet 100 at –171°C.

ΔK (MPa√m)	d*a*/dN (m/cycle)	ΔK (MPa√m)	d*a*/dN (m/cycle)	ΔK (MPa√m)	d*a*/dN (m/cycle)	ΔK (MPa√m)	d*a*/dN (m/cycle)
14.53	6.47E-08	9.10	1.57E-08	5.70	4.13E-09	3.58	8.08E-10
13.55	4.44E-08	8.51	1.22E-08	5.34	3.23E-09	3.34	5.94E-10
12.68	3.40E-08	7.99	9.75E-09	4.99	2.73E-09	3.12	4.41E-10
11.87	2.47E-08	7.41	8.37E-09	4.69	2.13E-09	2.94	3.11E-10
11.11	3.35E-08	6.96	6.96E-09	4.38	1.45E-09		
10.37	2.19E-08	6.53	5.70E-09	4.09	1.27E-09		
9.74	1.81E-08	6.12	5.18E-09	3.82	1.06E-09		

Table A3. Constant-K_{max} FCG data for C-250 at 24°C.

K_{max} = 22 MPa√m				K_{max} = 55 MPa√m			
ΔK (MPa√m)	d*a* /dN (m/cycle)	ΔK (MPa√m)	d*a* /dN (m/cycle)	ΔK (MPa√m)	d*a* /dN (m/cycle)	ΔK (MPa√m)	d*a* /dN (m/cycle)
15.47	6.25E-08	4.76	5.17E-09	38.94	4.32E-07	8.70	3.49E-08
14.43	5.77E-08	4.59	4.68E-09	36.76	3.90E-07	8.24	3.27E-08
13.42	5.58E-08	4.42	4.22E-09	34.79	3.74E-07	7.78	2.74E-08
12.39	4.48E-08	4.27	3.91E-09	32.99	3.60E-07	7.38	2.46E-08
11.53	3.72E-08	4.10	3.56E-09	31.13	3.26E-07	6.97	2.07E-08
10.67	3.19E-08	3.96	3.54E-09	29.55	3.01E-07	6.59	1.65E-08
10.33	2.78E-08	3.81	3.00E-09	27.90	2.77E-07	6.25	1.52E-08
9.96	2.49E-08	3.66	2.79E-09	26.44	2.62E-07	5.89	1.19E-08
9.59	2.17E-08	3.54	2.89E-09	24.96	2.40E-07	5.59	1.20E-08
9.26	2.15E-08	3.41	2.50E-09	23.66	2.18E-07	5.29	1.04E-08
8.93	1.88E-08	3.29	2.25E-09	22.36	2.05E-07	4.99	8.59E-09
8.60	1.61E-08	3.17	1.99E-09	21.12	1.90E-07	4.72	7.51E-09
8.31	1.46E-08	3.06	1.79E-09	20.03	1.78E-07	4.47	7.34E-09
8.00	1.36E-08	2.94	1.61E-09	18.94	1.63E-07	4.24	6.38E-09
7.70	1.25E-08	2.84	1.45E-09	17.88	1.46E-07	4.00	5.37E-09
7.43	1.10E-08	2.73	1.06E-09	16.90	1.31E-07	3.78	4.77E-09
7.15	1.14E-08	2.63	1.02E-09	16.03	1.21E-07	3.58	4.38E-09
6.90	1.00E-08	2.54	7.52E-10	15.17	1.11E-07	3.39	3.96E-09
6.64	9.09E-09	2.44	4.31E-10	14.34	9.70E-08	3.19	3.26E-09
6.40	7.75E-09	2.35	2.09E-10	13.57	8.87E-08	3.03	2.97E-09
6.16	7.40E-09	2.28	1.10E-10	12.84	8.11E-08	2.87	3.01E-09
5.94	7.63E-09	2.19	8.00E-11	12.08	7.31E-08	2.72	2.32E-09
5.73	6.14E-09	2.11	8.06E-11	11.48	6.56E-08	2.57	1.97E-09
5.51	6.15E-09	2.04	6.89E-11	10.88	5.63E-08	2.43	9.48E-10
5.31	6.03E-09			10.27	4.76E-08	2.17	5.96E-10
5.12	5.07E-09			9.72	4.45E-08	2.06	2.17E-10
4.94	5.36E-09			9.17	3.78E-08		

Table A4. Constant-K_{max} = 22 MPa√m fatigue crack growth data for C-250 at –171°C.

ΔK (MPa√m)	d*a* /dN (m/cycle)	ΔK (MPa√m)	d*a* /dN (m/cycle)	ΔK (MPa√m)	d*a* /dN (m/cycle)	ΔK (MPa√m)	d*a* /dN (m/cycle)
16.20	5.10E-08	9.30	1.37E-08	5.35	3.05E-09	3.07	4.61E-10
15.33	5.03E-08	8.80	1.17E-08	5.04	2.67E-09	2.89	4.01E-10
14.48	4.07E-08	8.33	9.76E-09	4.79	2.10E-09	2.74	2.52E-10
13.71	3.69E-08	7.89	8.49E-09	4.50	1.85E-09	2.59	2.21E-10
12.97	3.21E-08	7.45	7.45E-09	4.26	1.53E-09	2.45	2.60E-10
12.28	2.74E-08	7.05	6.46E-09	4.05	1.26E-09	2.32	2.00E-10
11.62	2.46E-08	6.66	5.31E-09	3.83	9.69E-10	2.19	1.33E-10
11.00	2.04E-08	6.30	4.62E-09	3.62	9.27E-10	2.08	1.97E-10
10.41	1.87E-08	5.97	4.08E-09	3.42	7.67E-10		
9.85	1.65E-08	5.64	3.72E-09	3.25	6.29E-10		

Table A5. Fatigue crack growth data for AerMet 100 at R = 0.5 and 24°C.

ΔK (MPa√m)	d*a*/dN (m/cycle)	ΔK (MPa√m)	d*a*/dN (m/cycle)	ΔK (MPa√m)	d*a*/dN (m/cycle)	ΔK (MPa√m)	d*a*/dN (m/cycle)
11.10	3.23E-08	17.81	1.08E-07	28.50	2.99E-07	45.67	8.52E-07
11.21	3.30E-08	17.96	1.11E-07	28.73	3.05E-07	46.08	9.30E-07
11.31	3.47E-08	18.13	1.13E-07	28.99	3.07E-07	46.48	9.11E-07
11.41	3.50E-08	18.29	1.14E-07	29.26	3.10E-07	46.93	9.18E-07
11.51	3.58E-08	18.45	1.17E-07	29.52	3.14E-07	47.32	9.65E-07
11.62	3.75E-08	18.61	1.20E-07	29.79	3.25E-07	47.75	1.02E-06
11.72	3.83E-08	18.78	1.20E-07	30.05	3.31E-07	48.17	1.10E-06
11.81	3.93E-08	18.95	1.25E-07	30.33	3.37E-07	48.66	1.04E-06
11.92	4.05E-08	19.13	1.26E-07	30.59	3.45E-07	49.04	1.07E-06
12.03	4.08E-08	19.28	1.28E-07	30.88	3.62E-07	49.48	1.15E-06
12.13	4.24E-08	19.46	1.32E-07	31.14	3.59E-07	49.94	1.25E-06
12.25	4.32E-08	19.64	1.36E-07	31.43	3.72E-07	50.37	1.29E-06
12.35	4.47E-08	19.79	1.37E-07	31.70	3.68E-07	50.84	1.28E-06
12.46	4.53E-08	19.97	1.47E-07	31.98	3.79E-07	51.28	1.37E-06
12.58	4.67E-08	20.13	1.42E-07	32.26	3.82E-07	51.73	1.37E-06
12.69	4.83E-08	20.31	1.47E-07	32.57	3.95E-07	52.22	1.44E-06
12.80	4.88E-08	20.50	1.49E-07	32.85	3.97E-07	52.70	1.59E-06
12.91	5.01E-08	20.67	1.55E-07	33.15	4.10E-07	53.14	1.62E-06
13.04	5.21E-08	20.85	1.59E-07	33.45	4.21E-07	53.61	1.47E-06
13.16	5.30E-08	21.07	1.61E-07	33.75	4.21E-07	54.10	1.55E-06
13.27	5.46E-08	21.23	1.62E-07	34.03	4.39E-07	54.57	1.73E-06
13.40	5.53E-08	21.42	1.61E-07	34.35	4.47E-07	55.07	1.74E-06
13.51	5.65E-08	21.63	1.71E-07	34.65	4.42E-07	55.54	2.06E-06
13.64	5.87E-08	21.81	1.66E-07	34.96	4.54E-07	56.09	2.31E-06
13.75	6.00E-08	22.02	1.78E-07	35.29	4.54E-07	56.60	2.32E-06
13.87	6.11E-08	22.22	1.79E-07	35.60	4.69E-07	57.06	2.31E-06
14.00	6.30E-08	22.40	1.82E-07	35.89	5.08E-07	57.57	2.41E-06
14.12	6.34E-08	22.59	1.87E-07	36.22	5.09E-07	58.08	3.02E-06
14.26	6.51E-08	22.80	1.89E-07	36.58	5.00E-07	58.60	3.14E-06
14.38	6.81E-08	23.01	1.90E-07	36.87	5.15E-07	59.14	3.79E-06
14.50	6.80E-08	23.21	1.99E-07	37.24	5.29E-07	59.65	4.23E-06
14.64	7.14E-08	23.41	2.00E-07	37.57	5.35E-07	60.20	3.85E-06
14.77	7.24E-08	23.63	2.02E-07	37.88	5.60E-07	60.75	4.10E-06
14.89	7.36E-08	23.84	2.11E-07	38.23	5.58E-07	61.29	4.71E-06
15.04	7.55E-08	24.06	2.10E-07	38.56	5.75E-07	61.83	4.47E-06
15.17	7.68E-08	24.27	2.15E-07	38.90	5.75E-07	62.38	4.90E-06
15.30	7.90E-08	24.49	2.17E-07	39.25	5.99E-07	62.93	5.85E-06
15.44	7.88E-08	24.72	2.23E-07	39.59	5.87E-07	63.57	7.26E-06
15.58	8.30E-08	24.92	2.29E-07	39.96	6.11E-07	64.11	1.13E-05
15.72	8.38E-08	25.17	2.34E-07	40.34	6.34E-07	64.78	1.36E-05
15.85	8.63E-08	25.39	2.32E-07	40.67	6.34E-07	65.51	2.34E-05
15.99	8.72E-08	25.60	2.49E-07	41.06	6.56E-07	66.10	2.54E-05
16.15	8.95E-08	25.83	2.41E-07	41.39	6.75E-07	66.62	1.96E-05
16.28	9.16E-08	26.07	2.48E-07	41.79	7.00E-07	67.07	1.50E-05
16.43	9.38E-08	26.29	2.54E-07	42.16	7.29E-07	67.60	1.82E-05
16.59	9.53E-08	26.52	2.57E-07	42.54	7.11E-07	68.30	2.26E-05
16.72	9.69E-08	26.77	2.57E-07	42.92	7.35E-07	68.89	2.64E-05
16.87	8.66E-08	27.01	2.64E-07	43.27	7.36E-07	69.70	3.71E-05
17.03	1.02E-07	27.26	2.68E-07	43.68	7.55E-07	70.39	2.94E-05
17.18	9.96E-08	27.50	2.84E-07	44.07	8.06E-07	70.86	4.11E-05
17.34	1.02E-07	27.73	2.74E-07	44.46	8.56E-07	71.54	6.09E-05
17.49	1.03E-07	28.00	2.88E-07	44.85	8.68E-07	72.49	8.30E-05
17.64	1.07E-07	28.23	2.98E-07	45.25	8.42E-07	73.60	9.69E-05

Table A6. Fatigue crack growth data for C-250 steel at R = 0.5 and 24°C.

ΔK (MPa√m)	d*a*/dN (m/cycle)	ΔK (MPa√m)	d*a*/dN (m/cycle)	ΔK (MPa√m)	d*a*/dN (m/cycle)	ΔK (MPa√m)	d*a*/dN (m/cycle)
13.64	6.12E-08	18.89	1.28E-07	26.17	2.29E-07	36.25	5.71E-07
13.84	6.29E-08	19.20	1.26E-07	26.59	2.40E-07	36.77	5.71E-07
14.05	6.37E-08	19.46	1.31E-07	26.95	2.42E-07	37.33	6.27E-07
14.26	6.65E-08	19.75	1.36E-07	27.35	2.61E-07	37.88	6.37E-07
14.47	6.83E-08	20.10	1.38E-07	27.76	2.67E-07	38.47	6.75E-07
14.69	6.85E-08	20.34	1.40E-07	28.18	2.90E-07	39.04	7.23E-07
14.92	7.14E-08	20.69	1.43E-07	28.59	2.81E-07	39.59	7.70E-07
15.14	7.61E-08	20.96	1.51E-07	29.02	2.88E-07	40.27	1.00E-06
15.36	7.87E-08	21.27	1.54E-07	29.45	2.93E-07	40.82	1.44E-06
15.59	8.07E-08	21.57	1.58E-07	29.91	3.05E-07	41.39	1.40E-06
15.82	8.42E-08	21.91	1.66E-07	30.35	3.15E-07	42.02	1.51E-06
16.05	8.88E-08	22.25	1.71E-07	30.78	3.30E-07	42.68	1.54E-06
16.28	9.13E-08	22.56	1.75E-07	31.24	3.32E-07	43.30	1.77E-06
16.53	9.28E-08	22.92	1.81E-07	31.70	3.49E-07	43.93	1.77E-06
16.79	9.41E-08	23.23	1.81E-07	32.19	3.85E-07	44.57	1.91E-06
17.03	9.97E-08	23.64	1.87E-07	32.67	3.93E-07	45.28	3.19E-06
17.28	1.04E-07	23.94	1.93E-07	33.19	3.88E-07	48.22	4.81E-06
17.55	1.06E-07	24.29	1.99E-07	33.66	3.89E-07	48.90	1.73E-05
17.80	1.10E-07	24.65	2.01E-07	34.14	4.10E-07	50.14	3.21E-05
18.08	1.12E-07	25.01	2.13E-07	34.69	4.53E-07		
18.35	1.18E-07	25.39	2.23E-07	35.20	5.31E-07		
18.61	1.16E-07	25.80	2.26E-07	35.72	5.64E-07		

Table A7. Fatigue crack growth data for C-250 at R = 0.5 (increasing ΔK) and –171°C.

ΔK (MPa√m)	d*a*/dN (m/cycle)	ΔK (MPa√m)	d*a*/dN (m/cycle)	ΔK (MPa√m)	d*a*/dN (m/cycle)	ΔK (MPa√m)	d*a*/dN (m/cycle)
11.18	1.83E-08	13.35	3.07E-08	15.94	5.74E-08	19.05	8.16E-08
11.26	2.24E-08	13.45	3.13E-08	16.07	4.89E-08	19.18	8.13E-08
11.34	2.44E-08	13.55	3.73E-08	16.18	5.45E-08	19.33	8.59E-08
11.43	1.71E-08	13.65	2.88E-08	16.30	6.15E-08	19.48	8.59E-08
11.52	2.17E-08	13.75	3.77E-08	16.42	5.07E-08	19.61	8.97E-08
11.61	2.41E-08	13.86	3.81E-08	16.54	5.56E-08	19.78	9.58E-08
11.69	2.26E-08	13.96	4.01E-08	16.68	6.61E-08	19.92	1.07E-07
11.78	2.34E-08	14.06	3.85E-08	16.79	6.29E-08	20.06	8.96E-08
11.87	2.36E-08	14.17	3.42E-08	16.92	5.99E-08	20.22	1.18E-07
11.96	2.32E-08	14.27	2.68E-08	17.05	5.70E-08	20.36	1.03E-07
12.03	2.47E-08	14.38	4.32E-08	17.17	6.25E-08	20.52	1.06E-07
12.13	1.97E-08	14.49	3.95E-08	17.30	6.51E-08	20.66	1.34E-07
12.21	2.68E-08	14.60	3.50E-08	17.42	6.93E-08	20.81	1.24E-07
12.31	2.72E-08	14.70	4.79E-08	17.56	6.03E-08	20.99	1.29E-07
12.41	2.79E-08	14.81	3.91E-08	17.69	6.10E-08	21.13	1.49E-07
12.50	3.83E-08	14.92	4.63E-08	17.82	6.91E-08	21.81	2.32E-07
12.58	2.54E-08	15.03	4.53E-08	17.95	7.35E-08	22.33	2.83E-06
12.67	3.23E-08	15.15	4.47E-08	18.08	7.76E-08	22.35	2.46E-07
12.77	2.86E-08	15.25	5.28E-08	18.23	7.54E-08	22.37	1.92E-07
12.87	3.11E-08	15.37	3.93E-08	18.36	6.95E-08	22.39	1.79E-07
12.97	2.81E-08	15.49	4.43E-08	18.50	7.49E-08	23.87	1.50E-05
13.06	2.89E-08	15.60	5.62E-08	18.62	7.86E-08		
13.16	3.03E-08	15.72	5.03E-08	18.77	8.47E-08		
13.26	3.02E-08	15.83	5.60E-08	18.90	8.65E-08		

Table A8. Fatigue crack growth data for AerMet 100 at R = 0.5 (increasing ΔK) and –171°C.

ΔK (MPa√m)	d*a* /dN (m/cycle)	ΔK (MPa√m)	d*a* /dN (m/cycle)	ΔK (MPa√m)	d*a* /dN (m/cycle)	ΔK (MPa√m)	d*a* /dN (m/cycle)
11.07	1.84E-08	12.88	3.17E-08	14.98	5.14E-08	17.42	7.55E-08
11.18	2.05E-08	12.99	3.34E-08	15.11	4.94E-08	17.59	7.61E-08
11.28	2.14E-08	13.11	3.41E-08	15.25	5.16E-08	17.74	7.95E-08
11.37	2.20E-08	13.22	3.58E-08	15.38	5.44E-08	17.91	8.69E-08
11.47	2.30E-08	13.35	3.70E-08	15.53	5.22E-08	18.07	8.95E-08
11.58	2.31E-08	13.46	3.83E-08	15.68	5.63E-08	18.23	9.51E-08
11.68	2.35E-08	13.59	4.42E-08	15.81	5.84E-08	18.39	9.51E-08
11.78	2.48E-08	13.71	3.78E-08	15.94	6.07E-08	18.55	9.63E-08
11.89	2.54E-08	13.83	4.10E-08	16.08	5.97E-08	18.72	1.08E-07
12.00	2.72E-08	13.96	4.59E-08	16.24	6.14E-08	18.88	1.10E-07
12.10	2.71E-08	14.08	4.01E-08	16.38	6.47E-08	19.05	1.21E-07
12.21	2.80E-08	14.21	4.23E-08	16.52	6.54E-08	19.23	1.38E-07
12.32	2.84E-08	14.33	4.43E-08	16.68	6.92E-08	19.42	1.32E-07
12.43	2.99E-08	14.47	4.26E-08	16.82	7.05E-08	19.56	1.36E-07
12.55	3.01E-08	14.59	4.73E-08	16.97	6.92E-08	19.75	1.98E-07
12.66	3.08E-08	14.73	4.45E-08	17.13	7.07E-08	19.91	3.20E-07
12.76	3.15E-08	14.85	4.81E-08	17.28	7.61E-08	20.10	3.35E-07

Table A9. Fatigue crack growth data for AerMet 100 at R = 0.5 (decreasing ΔK) and –171°C.

ΔK (MPa√m)	d*a* /dN (m/cycle)	ΔK (MPa√m)	d*a* /dN (m/cycle)	ΔK (MPa√m)	d*a* /dN (m/cycle)	ΔK (MPa√m)	d*a* /dN (m/cycle)
10.75	1.90E-08	8.46	9.11E-09	6.66	4.06E-09	5.24	1.68E-09
10.66	1.91E-08	8.38	8.44E-09	6.59	3.82E-09	5.18	1.60E-09
10.55	1.90E-08	8.31	8.01E-09	6.53	4.48E-09	5.14	1.42E-09
10.46	1.84E-08	8.23	8.20E-09	6.48	4.36E-09	5.09	1.33E-09
10.37	1.76E-08	8.16	8.22E-09	6.41	3.06E-09	5.05	1.45E-09
10.27	1.69E-08	8.09	7.65E-09	6.36	2.91E-09	5.01	1.42E-09
10.19	1.68E-08	8.02	7.76E-09	6.30	2.80E-09	4.96	1.38E-09
10.10	1.61E-08	7.94	7.42E-09	6.25	2.92E-09	4.91	1.63E-09
10.01	1.57E-08	7.88	7.21E-09	6.19	3.08E-09	4.87	1.94E-09
9.92	1.56E-08	7.81	6.85E-09	6.14	2.93E-09	4.83	1.13E-09
9.83	1.48E-08	7.73	6.83E-09	6.08	2.94E-09	4.79	9.73E-10
9.75	1.53E-08	7.67	6.43E-09	6.03	2.80E-09	4.74	1.25E-09
9.66	1.39E-08	7.60	6.48E-09	5.97	2.77E-09	4.70	1.08E-09
9.57	1.41E-08	7.52	6.01E-09	5.92	2.72E-09	4.65	6.06E-10
9.49	1.32E-08	7.46	6.91E-09	5.86	2.67E-09	4.62	8.25E-10
9.41	1.27E-08	7.40	6.66E-09	5.82	2.68E-09	4.58	8.50E-10
9.33	1.27E-08	7.34	4.89E-09	5.76	2.51E-09	4.53	4.36E-10
9.24	1.22E-08	7.27	5.29E-09	5.72	2.39E-09	4.50	8.55E-10
9.16	1.21E-08	7.21	5.24E-09	5.67	2.43E-09	4.46	8.13E-10
9.08	1.16E-08	7.14	5.25E-09	5.62	2.27E-09	4.41	6.28E-10
9.00	1.11E-08	7.07	4.96E-09	5.57	2.31E-09	4.38	5.70E-10
8.92	1.10E-08	7.01	4.89E-09	5.52	2.15E-09	4.35	6.12E-10
8.83	1.05E-08	6.95	4.53E-09	5.47	2.06E-09	4.30	6.15E-10
8.76	1.01E-08	6.89	4.45E-09	5.42	1.93E-09	4.27	6.36E-10
8.68	1.02E-08	6.83	4.38E-09	5.37	1.80E-09	4.22	6.44E-10
8.61	9.60E-09	6.77	4.18E-09	5.32	1.80E-09		
8.53	9.43E-09	6.71	4.18E-09	5.28	1.68E-09		

Table A10. Fatigue crack growth data for C-250 at R = 0.5 (decreasing ΔK) and –171°C.

ΔK (MPa√m)	d*a* /dN (m/cycle)	ΔK (MPa√m)	d*a* /dN (m/cycle)	ΔK (MPa√m)	d*a* /dN (m/cycle)	ΔK (MPa√m)	d*a* /dN (m/cycle)
12.47	2.74E-08	9.49	1.17E-08	7.22	5.02E-09	5.49	2.06E-09
12.40	2.85E-08	9.42	1.13E-08	7.16	5.19E-09	5.45	2.11E-09
12.30	2.52E-08	9.35	1.02E-08	7.12	4.92E-09	5.41	2.19E-09
12.21	2.61E-08	9.28	1.24E-08	7.06	5.06E-09	5.37	2.03E-09
12.12	2.77E-08	9.22	1.25E-08	7.01	4.83E-09	5.32	2.15E-09
12.02	2.47E-08	9.14	1.01E-08	6.95	4.62E-09	5.29	1.89E-09
11.94	2.26E-08	9.08	1.05E-08	6.91	4.56E-09	5.25	1.97E-09
11.85	2.49E-08	9.01	9.71E-09	6.85	4.58E-09	5.21	1.91E-09
11.76	2.27E-08	8.94	9.94E-09	6.81	4.14E-09	5.17	2.45E-09
11.67	2.61E-08	8.88	1.07E-08	6.75	4.40E-09	5.14	1.80E-09
11.58	2.30E-08	8.81	9.79E-09	6.70	3.87E-09	5.10	1.77E-09
11.51	2.22E-08	8.76	9.34E-09	6.66	4.13E-09	5.06	1.69E-09
11.41	2.36E-08	8.69	8.57E-09	6.60	4.01E-09	5.03	1.75E-09
11.34	2.02E-08	8.62	8.61E-09	6.56	3.61E-09	4.98	1.65E-09
11.25	1.95E-08	8.55	8.93E-09	6.50	3.88E-09	4.95	2.29E-09
11.17	2.06E-08	8.49	7.85E-09	6.46	3.46E-09	4.91	1.73E-09
11.09	1.99E-08	8.43	8.48E-09	6.41	3.31E-09	4.87	1.20E-09
11.01	1.90E-08	8.37	8.33E-09	6.37	3.50E-09	4.84	2.02E-09
10.92	1.98E-08	8.31	8.12E-09	6.31	3.41E-09	4.80	1.62E-09
10.84	1.79E-08	8.25	6.29E-09	6.27	3.41E-09	4.76	1.26E-09
10.76	1.78E-08	8.18	5.79E-09	6.23	3.25E-09	4.73	1.50E-09
10.68	1.97E-08	8.12	7.61E-09	6.18	3.32E-09	4.70	1.50E-09
10.59	1.50E-08	8.06	6.98E-09	6.14	2.89E-09	4.66	1.44E-09
10.53	1.58E-08	8.01	6.35E-09	6.08	3.04E-09	4.63	1.58E-09
10.45	1.61E-08	7.94	6.43E-09	6.04	3.12E-09	4.60	1.46E-09
10.36	1.54E-08	7.89	6.39E-09	6.00	3.59E-09	4.57	1.25E-09
10.30	1.63E-08	7.83	6.77E-09	5.95	2.45E-09	4.52	1.43E-09
10.22	1.60E-08	7.78	6.28E-09	5.91	2.72E-09	4.50	1.39E-09
10.14	1.59E-08	7.71	6.71E-09	5.86	2.64E-09	4.47	1.37E-09
10.05	1.54E-08	7.65	5.98E-09	5.83	2.69E-09	4.43	1.02E-09
10.00	1.28E-08	7.60	5.72E-09	5.79	2.52E-09	4.40	7.94E-10
9.92	1.33E-08	7.55	6.21E-09	5.74	2.52E-09	4.37	8.49E-10
9.85	1.36E-08	7.49	5.68E-09	5.70	2.40E-09	4.33	1.10E-09
9.78	1.35E-08	7.44	5.64E-09	5.65	2.47E-09	4.30	5.90E-10
9.70	1.34E-08	7.38	5.35E-09	5.61	2.46E-09	4.27	8.53E-10
9.64	1.39E-08	7.33	5.70E-09	5.58	2.67E-09	4.24	2.85E-10
9.56	1.27E-08	7.27	5.11E-09	5.53	2.77E-09	4.20	4.92E-10

Table A11. Fracture data obtained using the DCT specimen.

	fatigue pre-cracking				fracture		
	P_{max} (kN)	K_{max} (MPa√m)	*a* (mm)	*a* /W	temperature (^oC)	$P_{fracture}$ (kN)	K_{Ic} (MPa√m)
AerMet 100	3.59	4.7	63.5	0.561	24	97.22	128.4
	20.71	22.0	52.3	0.463	24	122.25	129.9
	19.97	22.0	53.7	0.475	24	120.67	133.0
	30.07	33.0	53.5	0.474	24	114.36	125.5
	24.95	27.5	53.7	0.475	24	119.50	131.7
	7.18	7.5	51.9	0.459	-171	33.54	34.9
	19.96	22.0	53.7	0.475	-171	31.18	34.3
	16.98	22.0	59.4	0.525	-171	36.65	47.4
	19.97	22.0	53.7	0.475	-171	31.89	35.1
	7.68	9.5	57.6	0.510	-171	31.94	39.3
C-250	19.06	22.0	43.3	0.460	24	84.33	97.4
	19.22	22.0	43.0	0.457	24	80.13	91.7
	19.67	22.0	42.4	0.450	24	82.18	91.9
	19.07	22.0	43.2	0.460	24	74.28	85.7
	14.12	16.5	43.7	0.464	24	71.92	84.1
	18.17	22.0	44.7	0.475	-171	41.92	50.8
	6.98	8.0	51.3	0.546	-171	32.56	37.3
	19.40	22.0	42.7	0.454	-171	39.65	45.0
	14.63	16.5	42.6	0.453	-171	43.57	49.1
	15.65	22.0	49.1	0.522	-171	33.85	47.6

Table A12. Fracture data obtained from MSCT specimens tested at 24^{o}C.

	fatigue pre-cracking					fracture		
	P_{max} (kN)	σ_{max} (MPa)	K_{max} (MPa√m)	*c* (mm)	*a* (mm)	$P_{fracture}$ (kN)	$\sigma_{fracture}$ (MPa)	K_c (MPa√m)
AerMet 100	50	517	19.3	1.01	1.06	120.5	1245	46.3
	50	517	17.1	0.82	0.88	124.3	1284	42.3
	50	517	20.4	1.12	1.20	117.9	1218	48.0
	40	414	17.1	1.15	1.19	122.3	1264	42.4
	50	517	23.7	1.47	1.56	118.3	1222	55.9
	50	517	30.3	2.37	2.38	109.5	1131	66.2
C-250	40	414	13.8	0.71	0.81	98.8	1021	32.0
	40	414	15.0	1.00	1.14	99.0	1023	38.1
	40	414	16.7	1.17	1.33	99.1	1024	41.5
	40	414	17.8	1.30	1.37	98.5	1018	43.6
	40	414	19.3	1.48	1.61	97.4	1006	46.3
	40	414	23.2	2.01	2.25	95.6	988	54.3

Table A13. Fracture data obtained from MSCT specimens tested at –171°C.

	fatigue pre-cracking					fracture		
	P_{max} (kN)	σ_{max} (MPa)	K_{max} (MPa√m)	*c* (mm)	*a* (mm)	$P_{fracture}$ (kN)	$\sigma_{fracture}$ (MPa)	K_c (MPa√m)
AerMet 100	50	517	28.3	2.06	2.12	127.1	1313	71.8
	50	517	19.6	1.06	1.15	144.7	1496	70.7
	40	414	15.2	0.94	0.87	147.5	1525	56.0
	40	414	19.7	1.61	1.64	133.7	1381	65.7
	40	414	14.1	0.94	0.97	147.1	1520	51.9
	40	414	21.6	1.75	1.69	131.9	1363	71.1
	40	414	17.5	1.25	1.33	142.9	1476	62.6
	40	414	16.7	1.19	1.08	147.1	1521	61.5
C-250	40	414	19.1	1.28	1.26	134.4	1389	64.3
	40	414	22.9	2.02	1.93	130.1	1344	74.4
	40	414	14.6	0.77	0.76	134.8	1393	49.3
	40	414	16.9	1.14	1.24	134.0	1385	56.7
	40	414	17.9	1.32	1.31	133.9	1384	60.0
	40	414	16.3	1.14	1.25	135.3	1398	55.0
	40	414	18.2	1.81	1.80	133.2	1376	60.4

Appendix B

For the example presented in the “Example of Damage-Tolerance Fatigue Analysis” section, “level 1” and “level 2” fatigue lives were calculated using the BASIC computer code listed below.

```
CLS
PRINT "Input KIc (MPa m^.5)"
INPUT KIc
PRINT "Input FCG threshold, DKth (MPa m^.5)"
INPUT DKth
PRINT "Input C"
INPUT c
PRINT "Input m"
INPUT m
PRINT "Input max stress (MPa)"
INPUT smax
PRINT "Input initial crack size (mm)"
INPUT aimm
PRINT "Input F"
INPUT F
PRINT "Input delta stress vibratory (MPa)"
INPUT Dsigv
PRINT "Input vibratory load cycles per polar"
INPUT DNv
PRINT "Input pitch buffet cyclic stress (MPa)"
INPUT Dsigp
PRINT "Input number of pitch buffet load cycles"
INPUT DNp
pi = ACOS(-1.0)
ai = aimm * .001
ms = (1 - .5 * m)
a = ai
af = (1 / pi) * (KIc / (F * smax)) ^ 2
count = 0

FOR j = 1 TO 200000
DKv = F * Dsigv * SQR(pi * a)
DKp = F * Dsigp * SQR(pi * a)
    IF (DKv < DKth) GOTO 50
a = (a ^ ms + (c * ms * DNv * (F * Dsigv * SQR(pi)) ^ m)) ^ (1 / ms)
50 PRINT
    IF (DKp < DKth) GOTO 60
a = (a ^ ms + (c * ms * DNp * (F * Dsigp * SQR(pi)) ^ m)) ^ (1 / ms)
60 PRINT
a = (a ^ ms + (c * ms * (F * smax * SQR(pi)) ^ m)) ^ (1 / ms)
count = count + 1
    IF (a > af) GOTO 100
NEXT j

100 PRINT "Failure during polar #", count
PRINT "Critical crack size =", af * 1000, "mm"
END
```

REPORT DOCUMENTATION PAGE

Form Approved
OMB No. 0704-0188

1. AGENCY USE ONLY (*Leave blank*)	2. REPORT DATE	3. REPORT TYPE AND DATES COVERED
	May 2002	Technical Memorandum

4. TITLE AND SUBTITLE
Evaluation of Fatigue Crack Growth and Fracture Properties of Cryogenic Model Materials

5. FUNDING NUMBERS
WU 706-21-11-10

6. AUTHOR(S)
John A. Newman, Scott C. Forth, Richard A. Everett, Jr., James, C. Newman, Jr., and William M. Kimmel

7. PERFORMING ORGANIZATION NAME(S) AND ADDRESS(ES)
NASA Langley Research Center
Hampton, VA 23681-2199

U.S. Army Research Laboratory
Vehicle Technology Directorate
NASA Langley Research Center
Hampton, VA 23681-2199

8. PERFORMING ORGANIZATION REPORT NUMBER
L-18179

9. SPONSORING/MONITORING AGENCY NAME(S) AND ADDRESS(ES)
National Aeronautics and Space Administration
Washington, DC 20546-0001
and
U.S. Army Research Laboratory
Adelphi, MD 20783-1145

10. SPONSORING/MONITORING AGENCY REPORT NUMBER
NASA/TM-2002-211673
ARL-TR-2725

11. SUPPLEMENTARY NOTES

12a. DISTRIBUTION/AVAILABILITY STATEMENT
Unclassified-Unlimited
Subject Category 26 Distribution: Nonstandard
Availability: NASA CASI (301) 621-0390

12b. DISTRIBUTION CODE

13. ABSTRACT *(Maximum 200 words)*
The criteria used to prevent failure of wind-tunnel models and support hardware were revised as part of a project to enhance the capabilities of cryogenic wind tunnel testing at NASA Langley Research Center. Specifically, damage-tolerance fatigue life prediction methods are now required for critical components, and material selection criteria are more general and based on laboratory test data. The suitability of two candidate model alloys (AerMet 100 and C-250 steel) was investigated by obtaining the fatigue crack growth and fracture data required for a damage-tolerance fatigue life analysis. Finally, an example is presented to illustrate the newly implemented damage tolerance analyses required of wind-tunnel model system components.

14. SUBJECT TERMS
Damage tolerance, Maraging steel, Wind tunnel model alloys, Cryogenic, Fracture
Fatigue crack growth

15. NUMBER OF PAGES
37

16. PRICE CODE

17. SECURITY CLASSIFICATION OF REPORT	18. SECURITY CLASSIFICATION OF THIS PAGE	19. SECURITY CLASSIFICATION OF ABSTRACT	20. LIMITATION OF ABSTRACT
Unclassified	Unclassified	Unclassified	UL